Journal of Sound and Vibration 566 (2023) 117929

Contents lists available at ScienceDirect

Journal of Sound and Vibration

journal homepage: www.elsevier.com/locate/jsvi

An efficient modelling technique for simulation of guided waves in delaminated composite and sandwich structures

Yuan Feng, Abdul Hamid Sheikh, Ching-Tai Ng *, Scott T. Smith

School of Architecture and Civil Engineering, The University of Adelaide, Adelaide, SA 5005, Australia

ARTICLE INFO

Keywords:
Laminated composite beam
Delamination modelling
Guided wave
Spectral finite element
Contact modelling

ABSTRACT

The paper presents a higher order laminate model with sub-lamination capability for simulating wave propagation within delaminated composite and sandwich beams. Each sub-laminate adopts cubic and quadratic through-thickness variation for axial and transverse displacement, respectively. This is achieved by taking displacements at external surfaces, which are beneficial for connecting sub-laminates, used to model multilayered structures by stacking them in the thickness direction without additional treatment. The model has the flexibility to achieve the desired level of accuracy and computational efficiency by using a suitable sub-lamination scheme. The delamination can be inserted conveniently between two sub-laminates stacked one over the other. The effect of contact within delamination regions is also incorporated in this model to capture higher harmonics induced by a clapping mechanism produced during delamination closing. The model is implemented within a framework of spectral finite elements in the time-domain. The accuracy and computational efficiency of the model are thoroughly checked by solving numerical examples of wave propagation within intact/delaminated composite/sandwich beams. Detailed finite element (FE) models used to produce results for validation show that the proposed model can save more than 90% of computing time and memory compared to detailed FE modelling to achieve similar level accuracy. The model is finally utilised to investigate the influence of delamination sizes and location on the wave response of sandwich beams.

1. Introduction

Structural members comprised of composite laminates are used in aerospace, civil, mechanical, and marine engineering activities because of their attractive properties such as high strength-to-weight and stiffness-to-weight ratios, durability, and manufacturing flexibility. The composite laminates are made by stacking multiple fibre-reinforced polymer (FRP) plies/laminas having bonded connections. A special type of composite laminate that exploits lightweight features is a sandwich structure where an ultra-lightweight thick inner core layer with relatively low strength and stiffness is sandwiched between two thin composite face sheets [1].

Delamination is one of the common damages found in laminated composite structures at the interfaces between plies, which can grow and lead to a considerable reduction of stiffness and strength of these structures. A damage detection technique is therefore essential to obtain an early warning to prevent catastrophic failure of structures. Damage detection using high frequency ultrasonic guided waves is one of the non-destructive techniques, which has attracted significant attention in recent years since its small wavelength can help to detect even small size damage. A number of studies have been undertaken on its application in metal/isotropic

* Corresponding author.
E-mail address: alex.ng@adelaide.edu.au (C.-T. Ng).

https://doi.org/10.1016/j.jsv.2023.117929
Received 21 March 2023; Received in revised form 6 July 2023; Accepted 7 July 2023
Available online 10 July 2023

[2–7] and composite [8–11] structures. Compared to isotropic metallic structures, the behaviour of guided waves in multilayered composite structures is much more complex due to material anisotropy. Therefore, precise modelling of guided wave propagation within these composite structures is needed to correctly understand the behaviour of waves when interacted with the damage. Thus, it can support the development of a reliable damage detection technique for composite structures using ultrasonic guided wave data. So far, various techniques have been employed to simulate wave propagation in composite structures although an accurate technique capable of detecting small damages in these structures is limited. Few analytical models [12–14] can provide good solutions, but they are limited to modelling structures and defects with simple geometries. The other technique is the use of 3D finite element (FE) modelling [15–17], which became very popular since it can conveniently simulate complex structural and damage geometries. However, the modelling of high-frequency waves having small wavelengths for detecting small damage needs a very fine FE meshing that in turn leads to a high computational cost that may not be affordable in all situations.

In order to reduce the computational burden of conventional 3D FE models, some researchers attempted to develop spectral finite element (SFE) based models. The initial development of such models was primarily frequency domain although the SFE in time domain was subsequently found to be convenient for the damage detection problem. In this case (SFE), a single element possesses a greater number of nodes for accommodating higher order interpolation/shape functions, which helps to capture high frequency waves effectively. However, it is to be noted that the interpolation functions based on usual nodal systems with regular spacing can produce significant errors near the edge nodes and this is known as the Runge phenomenon [18]. This issue has been successfully overcome by using non-uniform nodal locations obtained from the Gauss-Lobatto-Legendre (GLL) function where nodes are densely located near the element edges [19]. Compared to traditional FE modelling, SFE is found to converge faster and provides higher computational efficiency for the simulation of wave propagation [18]. A time-domain based SFE was developed and successfully used for simulating wave propagation in composite structures [20–22].

One of the key features behind computational efficiency of SFE is the use of laminated models for idealising the deformation of composite laminates as plate or beam bending problems (not 3D model). These include the class laminate theory (CLT), most primitive but popular in other application for computationally efficient, where the effect of shear deformation is neglected. Since the effect of shear deformation is significant in laminated composites due to low transverse shear modulus, CLT underestimates the wave phase velocities that leads to fail in simulating guided waves [23]. The first order shear deformation theory (FSDT) [24–27] became successful in simulating the wave propagation problem with little extra computational cost and complexity. Thus, FSDT is mostly used in existing SFE-based models, which can properly simulate the fundamental mode of waves but inadequate to simulate higher mode of waves [28] necessary for small size damage detection. In addition, FSDT neglects cross-sectional warping and its effect needs to be compensated using a parameter known as the shear correction factor, whose estimation is much more challenging for laminated composites [29]. This has inspired the development of higher order shear deformation theory (HSDT) based models [28,30,31] considering the effect of nonlinear sectional warping using higher order through-thickness variation of in-plane displacements. This has helped to eliminate shear correction factors, while improving the solution accuracy including a bit of improvement in simulating higher frequency waves.

These laminate theories (CLT, FSDT, and HSDT) belong to the group of equivalent single layer theory (ESLT) where variations of displacements over the laminate thickness are expressed in terms of continuous polynomial functions that take their weighting parameters at a single reference plane. Thus, the derivatives of these functions expressing the displacements provide continuous variations of strains over the laminate thickness. However, the transverse strains show a discontinuity at the ply interfaces in practice due to an abrupt change of material properties of adjacent layers. Thus, ESLT-based models are not only incapable of simulating high frequency waves satisfactorily, but they are also inadequate for accurately simulating the usual fundamental mode of waves in thick multilayered composites structures or sandwich structures with high material heterogeneity. Moreover, incorporation of de-laminations in an ESLT-based model is problematic. Some researchers [25,32] attempted to solve the issue by using two sets/layers of elements to model the delaminated region (one set of elements above the delamination and the other set below the delamination) while the intact portion is modelled with a single layer of elements. This technique appeared to provide a simple solution of the problem although it violated some aspects such as reference plane mismatch of elements at the transition between intact and delaminated regions that gave an ill representation of the actual problem. Moreover, these models did not consider the effect of contact (a nonlinear phenomenon) in the delamination region to avoid unrealistic interpenetrations of upper and lower portions of the delamination. This is crucial as mentioned in some studies [33–35], specifically in some problems such as detection of small damages using higher harmonics caused by clapping of the upper portion of a delamination with its lower portion that is ensured by using contact between them.

In order to eliminate the limitations of ESLT, Rekatsinas et al. [36] used a layer-wise (LW) based laminate theory to develop a SFE model for simulating wave propagation in composite and sandwich structures with no delamination. The LW theory provides a better representation of the variations of displacements in the thickness direction by using unknowns at all layer interfaces, which can also represent the interfacial transverse strain discontinuities successfully. This helped to achieve a significant improvement of the prediction capability. Compared to typical 3D FE modelling, LW theory-based models are relatively better in terms of computational cost. This is due to the element length (LW) not being restricted by the ply thickness, unlike FE models where the element aspect ratio needs to be restricted within a certain limit. However, the unknowns in a LW model are dependant on the number of layers/interfaces, which may not be preferred and the computational cost can still be high for modelling multilayered composites. This has inspired Kapuria et al. [37,38] to develop a zigzag (ZZ) laminate theory based SFE, where the unknowns at all interfaces are replaced by the unknowns at one reference plane by using inter-laminar stress (transverse) continuity conditions. The accuracy of this computationally efficient model (ZZ) is not poor, but those mentioned ZZ theory-based model [37,38] demands a C^1 continuous displacement field in its FE implementation which is a challenging issue. Moreover, incorporation of de-laminations within a typical ZZ model is another issue if it

(ZZ model) is applied for modelling the laminate unless it (whole laminate) is divided into sub-laminates and apply ZZ models separately to the individual sub-laminates. This is not addressed in the above mentioned ZZ theory based SFE [37,38] as the research is focused on wave propagation of intact laminates. Though the issue of C^1 continuous finite element formulation has been addressed in some studies [39–41] using different strategies along with other advancements (e.g., transverse deformability), these models are neither applied to wave propagation problems nor modelled de-laminations. It is possible to extend one of these techniques to the address the proposed problem, but this option is not chosen since the incorporation of delamination will be cumbersome. Thus, a different strategy is adopted in this study to develop a model that can address all the above-mentioned issues with no major complexities for successfully simulating the propagation of guided waves within delaminated composite and sandwich structures considering the effect of contact.

In this study, a pure displacement-based higher order laminate model having sub-lamination modelling [42] capability is developed for simulation of wave propagation within delaminated composite and sandwich beams. Within a sub-laminate, cubic and quadratic functions (polynomials) are used to achieve a higher order approximation of the through-thickness variation of axial and transverse displacements, respectively. These functions are expressed in terms of unknown displacements at exterior (top and bottom) surfaces of the sub-laminate. For an accurate simulation of a multilayered beam, it can be modelled by stack multiple sub-laminates in its thickness direction where the unknown displacement at the exterior surfaces facilitates to connect the sub-laminates conveniently and does not need any additional transformations. This modelling strategy also allow to conveniently accommodate a delamination between two adjacent sub-laminates stacked in the thickness direction. In this scenario, a contact algorithm is used to link the unknown displacements at the two surfaces of the delamination where they are disconnected when delamination opens while connected with high stiffness springs during delamination closing. The model can accommodate a portion of the beam thickness having multiple layers with no delamination into one sub-laminate to improve computation efficiency without compromising solution accuracy.

A C° continuous SFE model is developed based on this laminate theory and the model is implemented by developing a code in MATLAB while keeping as general as possible. The model permits the accommodation of any number of nodes in an element automatically in order to achieve any level of precision with reference to discretisation along the beam length. Similarly, the any level of discretisation along thickness direction can be achieved by choosing the appropriate number of higher order sub-laminates. This can achieve a highly accurate solution with higher computational cost or a moderately accurate solution with computation efficiency. That is, the model has the flexibility of trading of between accurate and computational cost. The performance of the model is first validated by simulating wave propagation in laminated beams with/without delamination. In the absence of suitable results available in the literature for validation, numerical results are generated by simulating the same beam problems using detailed FE modelling (expensive model) employing a reliable FE package code (ABAQUS). After a successful validation of the model, it is utilised to investigate the influence of delamination size and location on the wave responses of sandwich beams.

2. Model formulation

2.1. Higher order beam theory

The mathematical formulation for the proposed theory to model high frequency wave propagation within multilayered laminated beams is presented in this section. The model has sub-lamination modelling capability that permits to simulate the entire laminated beam by stacking a few sub-laminates each consisting of a couple of physical layers/plies (Fig. 1). A higher order through-thickness deformation kinematics is introduced for modelling each sub-laminate for accurately capturing high frequency waves needed to detect small-scale defects. This higher order sub-laminate model (HOSLM) can also function like an equivalent single layer model, where the whole structure is simulated with one sub-laminate, or like a typical layer-wise model by taking every layer as a sub-laminate.

The deformation of a sub-laminate is assumed to have a two-dimensional (2D) plane stress condition in the x-z plane (see Fig. 1a). According to the HOSLM, the through-thickness variations for axial (u) and transverse (w) displacements (primary displacements in 2D plane) of a sub-laminate are approximated as follows

$$u = u_0 - z\theta + z^2\alpha + z^3\beta \tag{1}$$

$$w = w_0 + z\gamma + z^2\delta \tag{2}$$

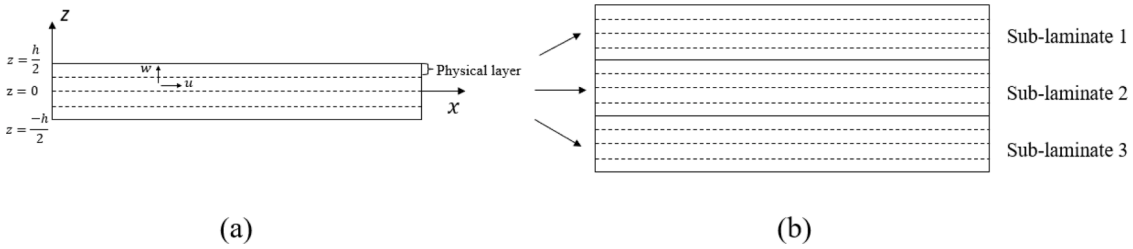

Fig. 1. (a) Typical higher order sub-laminate model (HOSLM) based sub-laminate with four physical layers, (b) Twelve-layered beam modelled by three sub-laminates.

where u_0 and w_0 are mid-plane axial and transverse displacements, respectively, and θ is the rotation of the sectional plane normal to x axis Fig. 1a) passing through the mid-plane of the sub-laminate (1D displacement field). The terms $\alpha, \beta, \gamma, \delta$ higher order variations of u and w. As these terms are non-physical parameters, they are replaced in terms of physical quantities (axial and transverse displacements) incorporating at the sub-laminate top (u_T, w_T) and bottom (u_B, w_B) surfaces. This is done by substituting Eqs. (1) and ((2) at $z = \frac{h}{2}$ and $z = -\frac{h}{2}$ (see Fig. 1a) that leads to $\alpha = \frac{2(u_T+u_B-2u_0)}{h^2}$, $\beta = \frac{4(u_T-u_B+h\theta)}{h^3}$, $\gamma = \frac{w_T-w_B}{h}$, $\delta = \frac{2(w_T+w_B-2w_0)}{h^2}$. The displacement fields can therefore be defined as:

$$u = A_u u_0 + B_u \theta + C_u u_T + D_u u_B \tag{3}$$

$$w = A_w w_0 + B_w w_T + C_w w_B \tag{4}$$

where $A_u = \frac{h^2-4z^2}{h^2}$, $B_u = \frac{4z^3-h^2 z}{h^2}$, $C_u = \frac{2hz^2+4z^3}{h^3}$, $D_u = \frac{2hz^2-4z^3}{h^3}$, $A_w = \frac{h^2-4z^2}{h^2}$, $B_w = \frac{hz+2z^2}{h^2}$, $C_w = \frac{2z^2-hz}{h^2}$. It should be noted that the incorporation of displacements at the top and bottom surfaces (u_T, w_T, u_B, w_B) facilitates easy connection of the sub-laminates without any additional treatment. Moreover, these displacements at external surfaces are beneficial for conveniently modelling delamination in composite laminates (details provided in Section 2.3). In addition to the adopted higher order variations of displacements (HOSLM), the capability of stacking multiple HOSLM-based sub-laminates helps to improve the modelling accuracy.

2.2. Governing equation of motion

The equation of motion for a dynamic system can be derived using the Lagrange equation. It can be expressed as:

$$\frac{d}{dt}\left\{\frac{\partial L}{\partial \dot{\boldsymbol{\Delta}}}\right\} - \left\{\frac{\partial L}{\partial \boldsymbol{\Delta}}\right\} + \left\{\frac{\partial R}{\partial \dot{\Delta}}\right\} = 0 \tag{5}$$

where L (= T - V) is the Lagrangian consisting of kinetic energy (T) and potential energy (V) that is dependant on strain energy U and work done by external load W_e ($V = U$-W_e), R is the dissipation potential to capture damping, $\boldsymbol{\Delta}$ is the unknown displacement vector (details will be shown later in this section), t is the time, and $\dot{\Delta}$ is the velocity vector ($d/dt\ \boldsymbol{\Delta}$). The key components ($V$, T, R) of Eq. (5) can be expressed as

$$\begin{cases} V = \frac{1}{2}\iint \boldsymbol{\varepsilon}^T \boldsymbol{\sigma} dx dz - \int \left(u q_x + w q_z\right) dx \\ T = \frac{1}{2}\iint \left(\rho_x \dot{u}^2 + \rho_z \dot{w}^2\right) dx dz \\ R = \frac{1}{2}\iint \left(\mu_x \dot{u}^2 + \mu_z \dot{w}^2\right) dx dz \end{cases} \tag{6}$$

where $\boldsymbol{\varepsilon}$ is the strain vector, $\boldsymbol{\sigma}$ is the stress vector, $q_x = q_x(x,t)$ is a distributed axial load and $q_z = q_z(x,t)$ is a distributed transverse load (similarly applicable to point load and other loads), ρ is the mass density (subscripts show directions) and μ is the damping coefficient. Displacements with dots in the equations represent their time derivatives. Note also that q_x and q_z act at the top, bottom or mid-surfaces of the beam and having no variations along the z axis. Though a generic treatment for the load is shown in this section, the present study primarily used point loads in the form of high frequency impulse, such as the Hann windowed tone burst (see the details later). The different responses (displacements, velocities, strain, and stresses) associated with Eq. (6) are presented below in convenient forms for deriving the equation of motion from Eq. (6).

Eqs. (3) and (4) can be used to express the primary displacements (u, w) in terms of 1D displacement field $\mathbf{f}^T = [u_0 \quad \theta \quad u_T \quad u_B \quad \omega_0 \quad \omega_T \quad \omega_B]$ and a sectional matrix $\mathbf{H_d}$ dependant on z as

$$\begin{Bmatrix} u \\ w \end{Bmatrix} = \mathbf{H_d}\mathbf{f} \tag{7}$$

where

$$\mathbf{H_d} = \begin{bmatrix} A_u & B_u & C_u & D_u & 0 & 0 & 0 \\ 0 & 0 & 0 & 0 & A_w & B_w & C_w \end{bmatrix} \tag{8a}$$

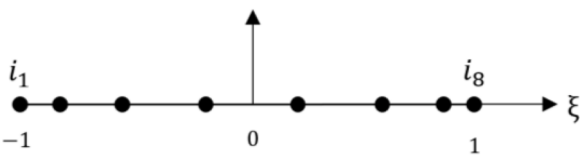

Fig. 2. Location of Gauss-Lobatto-Legendre (GLL) nodes of typical spectral finite element (SFE) with eight nodes.

To model beams under high frequency waves to capture small-scale defects, SFE with higher order approximations of the x directional displacement components of $\mathbf{f}$ are used. For this purpose, GLL nodes are used to improve the accuracy of interpolations compared to usual FE interpolation functions with equispaced nodes that may accumulate errors at the two ends (Runge's phenomenon) for higher order approximations. Fig. 2 shows the location of GLL nodes of a typical case with eight nodes but it can also be any other number of nodes n.

As the proposed laminate model can be implemented with C° FE formulation, all seven displacement components of $\mathbf{f}$ are interpolated with the same number of GLL nodes n per element where the k-th displacement component f^k of $\mathbf{f}$ can be expressed as

$$f^k = \sum_{i=1}^{n} N_i \Delta_i^k \tag{8b}$$

where N_i is the interpolation function corresponding to node i and Δ_i^k is the nodal displacement at node i corresponding to f^k. The location of GLL nodes $\xi_i \in [-1, 1]$ can be obtained by solving a set of equations $(1-\xi_i^2)L'_{n-1}(\xi_i) = 0$ for $i \in 1, \ldots, n$ where L'_{n-1} is the derivative of $(n\text{-}1)^{\text{th}}$ order Legendre polynomial [18] with respect to ξ, and n is the total number of GLL nodes within each element. Once the locations of GLL nodes are obtained, the expressions of N_i are determined using Lagrangian polynomials [43].

Eq. (8) is then substituted into Eq. (7) to express the 1D displacement vector $\mathbf{f}$ in terms of the nodal displacement vector $\mathbf{\Delta}$ consisting of m ($=n \times 7$) nodal unknowns (Δ_i^k) as

$$\begin{Bmatrix} u \\ w \end{Bmatrix} = \mathbf{H_d B_d \Delta} \tag{9}$$

where $\mathbf{B_d}$ consists of 1D shape functions N_i.

Following a similar procedure, the time derivative of Eqs. (3) and (4), providing velocities at any point in the 2D plane within a sub-laminate, can be expressed in terms of the nodal velocity vector $\dot{\Delta}$ as

$$\begin{Bmatrix} \dot{u} \\ \dot{w} \end{Bmatrix} = \mathbf{H_v B_v} \dot{\Delta} \tag{10}$$

where $\mathbf{B_v} = \mathbf{B_d}$ and $\mathbf{H_v} = \mathbf{H_d}$.

The primary strain vector $\boldsymbol{\varepsilon}$ in the 2D plane can be written in terms of derivatives of u and w, and with the aid of Eqs. (3) and (4) it can be decoupled into a z dependant sectional matrix $\mathbf{H}$ and x dependant 1D strain vector $\bar{\varepsilon}$ as

$$\boldsymbol{\varepsilon} = \begin{Bmatrix} \varepsilon_x \\ \varepsilon_z \\ \gamma_{xz} \end{Bmatrix} = \begin{Bmatrix} \dfrac{\partial u}{\partial x} \\ \dfrac{\partial w}{\partial z} \\ \dfrac{\partial u}{\partial z} + \dfrac{\partial \omega}{\partial x} \end{Bmatrix} = \mathbf{H}\bar{\varepsilon} \tag{11}$$

where

$$\mathbf{H} = \begin{bmatrix} 0 & 0 & 0 & 0 & A_u & B_u & C_u & D_u & 0 & 0 & 0 & 0 & 0 & 0 \\ 0 & 0 & 0 & 0 & 0 & 0 & 0 & 0 & \dfrac{\partial A_w}{\partial z} & \dfrac{\partial B_w}{\partial z} & \dfrac{\partial C_w}{\partial z} & 0 & 0 & 0 \\ \dfrac{\partial A_u}{\partial z} & \dfrac{\partial B_u}{\partial z} & \dfrac{\partial C_u}{\partial z} & \dfrac{\partial D_u}{\partial z} & 0 & 0 & 0 & 0 & 0 & 0 & 0 & A_w & B_w & C_w \end{bmatrix} \tag{12}$$

$$\bar{\varepsilon}^T = \begin{bmatrix} u_0 & \theta & u_T & u_B & \dfrac{\partial u_0}{\partial x} & \dfrac{\partial \theta}{\partial x} & \dfrac{\partial u_T}{\partial x} & \dfrac{\partial u_B}{\partial x} & \omega_0 & \omega_T & \omega_B & \dfrac{\partial w_0}{\partial x} & \dfrac{\partial w_T}{\partial x} & \dfrac{\partial w_B}{\partial x} \end{bmatrix} \tag{13}$$

The strain vector (Eq. (13)) is dependant on seven 1D displacement components appearing in $\mathbf{f}$.

Eq. (8) is then substituted into Eq. (13) to express the one-dimensional strain vector in terms of the nodal displacement vector $\mathbf{\Delta}$ as:

$$\bar{\varepsilon} = \mathbf{B}\Delta \tag{14}$$

where the strain-displacement matrix $\mathbf{B}$ consists of 1D shape functions and their derivatives.

A typical composite ply within a laminated beam or sub-laminate is idealized as a homogeneous orthogonal material layer and its 3D stress-strain (σ - ε) relationship in its off-axis (material axis) system (1–2–3) can be written as: $\boldsymbol{\sigma}_{\mathbf{off}} = \mathbf{Q}\boldsymbol{\varepsilon}_{\mathbf{off}}$ where the 6×6 constitutive matrix $\mathbf{Q}$ is depended on direction-dependant elastic modulus (E_1, E_2, E_3), shear modulus (G_{12}, G_{23}, G_{31}) and Poisson's ratio (ν_{12}, ν_{23}, ν_{31}) [44]. For a multi-layered laminate/sub-laminate, the stress-strain relationship of individual layers having different fibre orientations needs to be expressed in terms of a common axis system of the laminate in order to combine their contributions. This is done by the coordinate transformation of the constitutive relationship of individual layers to express that in the laminate axis (on-axis) system (x-y-z) using a transformation matrix $\mathbf{T}$ dependant on ply/fibre orientations (θ) as [44]

$$\boldsymbol{\sigma}_{\mathbf{on}} = \overline{\mathbf{Q}}\boldsymbol{\varepsilon}_{\mathbf{on}} \tag{15}$$

Since the sub-laminate is assumed to have a plane stress condition in the x-z plane, $\sigma_y = \tau_{xy} = \tau_{yz} = 0$. To implement this condition, Eq. (7) is inverted to appear the stress components on the right-hand side that helped to conveniently reduce the size of the system of equations from 6 to 3. The reduced form of this equation is inverted again to arrive at the final form of the 2D constitutive relationship of a composite ply as:

$$\boldsymbol{\sigma} = \mathbf{D}\varepsilon \tag{16}$$

Systematically substituting Eqs. (9)–(11), (14) and (15) into Eq. (6), potential energy V and kinetic energy T can be expressed as

$$\begin{cases} V = \frac{1}{2}\boldsymbol{\Delta}^T \int \mathbf{B}^T \mathbf{D}_{\mathbf{K}} \mathbf{B} \Delta dx - \boldsymbol{\Delta}^T \int \mathbf{B}_{\mathbf{d}}^T \overline{\mathbf{q}} dx = \frac{1}{2}\boldsymbol{\Delta}^T K \Delta - \boldsymbol{\Delta}^T P \\ T = \frac{1}{2}\dot{\Delta}^T \left(\int \mathbf{B}_{\mathbf{v}}^T \mathbf{D}_{\mathbf{m}} \mathbf{B}_{\mathbf{v}} dx \right) \dot{\Delta} = \frac{1}{2}\dot{\Delta}^T M \dot{\Delta} \end{cases} \tag{17}$$

where $\mathbf{K}$ is the stiffness matrix, $\mathbf{P}$ is the load vector, $\mathbf{M}$is the mass matrix, $\mathbf{D}_{\mathbf{K}} = \int \mathbf{H}^T \mathbf{D} \mathbf{H} dz$, $\overline{\mathbf{q}} = \mathbf{H}_{\mathbf{d}}^T \begin{bmatrix} q_x & 0 \\ 0 & q_z \end{bmatrix} \mathbf{H}_{\mathbf{d}}$, and $\mathbf{D}_{\mathbf{m}} = \int \mathbf{H}_{\mathbf{v}}^T \begin{bmatrix} \rho_x & 0 \\ 0 & \rho_z \end{bmatrix} \mathbf{H}_{\mathbf{v}} dz$. It is to be noted that $\overline{\mathbf{q}}$ needs not be integrated over z as the load can only have distribution along x and not along z. Thus,$\mathbf{H}_{\mathbf{d}}$ used in the above equation should be substituted with a contact value of z depending on the position of the load.

In a similar manner, the dissipation potential can be derived using Eqs. (6) and (10) as

$$R = \frac{1}{2}\dot{\Delta}^T \mathbf{C} \dot{\Delta} \tag{18}$$

where $\mathbf{C}$ is the damping matrix and can be expressed in terms of $\mathbf{H}_{\mathbf{v}}$, $\mathbf{B}_{\mathbf{v}}$, μ_x,and μ_z. However, due to the challenges associated with direct measurement of the damping coefficient, the concept of Rayleigh damping is used in this study. This helps to express the damping matrix in the proportion of the stiffness and mass matrices as $\mathbf{C} = a_0\mathbf{M} + a_1\mathbf{K}$ where the coefficients a_0 and a_1 can be evaluated using natural frequencies and the specified damping ratio with respect to the critical damping coefficient of the structure (details are available in a standard text [45]).

Substitution of Eqs. (17) and (18) into Eq. (5) produces the following governing equation of motion:

$$\boldsymbol{K\Delta} + \mathbf{C}\dot{\Delta} + \mathbf{M}\ddot{\Delta} = \mathbf{P} \tag{19}$$

Though the above equation is derived using an element of a sub-laminate, the same form of the equation is applicable for the whole structure by assembling the contribution of all components of the equation from all elements and their sub-laminates. For the intact portion of the laminate, the connection between two adjacent sub-laminates placed one over the other along the thickness direction can be simply achieved by taking the nodes at the bottom surface of the upper sub-laminate and the nodes at the top surface of the lower sub-laminate as common nodes.

The proposed HOSLM has significant benefits in modelling delaminations due to the presence of nodes at the two external surfaces (top/bottom) of a sub-laminate. Delamination can be easily inserted between two HOSLM-based sub-laminates by taking double sets of nodes with no physical gap between them (See Fig. 3). In that case, one set of nodes is attached to the bottom surface of the upper sub-laminate and the other set of nodes is attached to the top surface of the lower sub-laminate. Propagation of guided waves with a damaged/delaminated structure is often classified into two categories: linear waves and non-linear waves. For linear waves, the upper and lower sets of nodes are assumed to behave independently with no connection between them in order to simplify the analysis. However, there might be interactions between these node sets in reality and it can be used for nonlinear wave simulation due to contact effects at the delamination. For such simulation, these two sets of nodes are disconnected during delamination opening under tensile loading while a contact mechanism is incorporated between them during delamination closing under compressive loading that avoids a possible interpenetration of these adjacent sub-laminates. The contact is simulated by inserting zero length penalty springs between

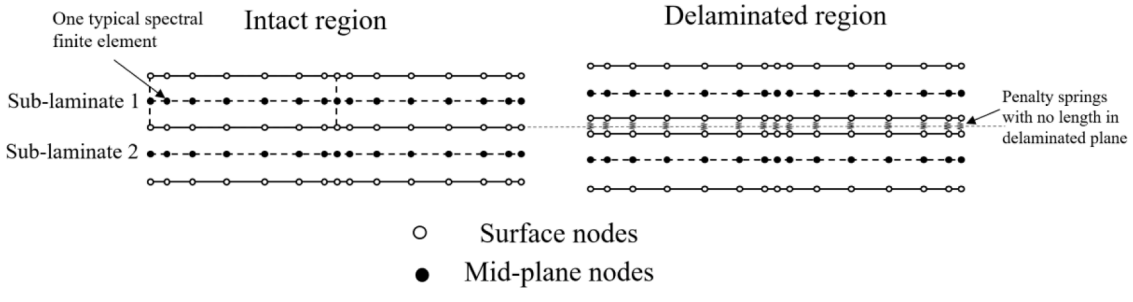

Fig. 3. Modelling intact and delamination regions with spectral finite elements (SFEs).

these two sets of nodes, where the stiffness of these springs is switched to zero to deactivate them during delamination opening. This is controlled by checking the values of w of the two sets of nodes, although it introduces a nonlinearity in the form of contact, which is solved iteratively following the successive approximation technique. In order to avoid any numerical disturbance and achieve converged results, the value of the penalty stiffness should be chosen in a range, recommended by Bathe [43], which should be around 10^3 times of the diagonal element of the structural stiffness matrix corresponding to the degree of freedom restrained by the spring.

2.3. Solution of the governing equation

Eq. (19) can be solved directly following a time integration technique, such as the Newmark beta method [18], but such an implicit time integration can take more computing time compared to an explicit time integration technique. In that case, the above equation is rearranged as

$$\mathbf{M}\ddot{\Delta} = \mathbf{P} - \boldsymbol{K}\boldsymbol{\Delta} - \mathbf{C}\dot{\Delta} = \mathbf{P} - \mathbf{P_K} - \mathbf{P_C} \tag{20}$$

where the solution process operates on the mass matrix appeared on the left-hand side of the equation considering contributions of stiffness and damping on its right-hand side in the form of corresponding load vectors $\mathbf{P_K}$ and $\mathbf{P_C}$. The explicit time integration technique uses lumped mass matrix with non-zero diagonal elements only that facilitates decoupling the multiple degrees of freedom (DOF) system into several single DOF problems. This is the key to improve computational efficiency. It also does not need an operation on the big stiffness and damping matrices of the structure as their contributions are incorporated in the form of corresponding load vectors evaluated at the element/sub-laminate levels and assembled them to get $\mathbf{P_K}$ and $\mathbf{P_C}$. The central difference with respect to time is used to solve the individual single DOF based equations to obtain the nodal displacement, velocity and acceleration of the beam.

It is to be noted that a diagonal mass matrix can be achieved by using nodal quadrature based spatial integration of the mass matrix (Eq. (17)) taking GLL nodes as integration points. This is valid for a usual SFE formulation, but it is not applicable to the present model due to higher order couplings between translational and rotational DOFs appeared in defining the through-thickness deformational kinematics of the beam. However, an alternative technique is used in the present scenario to diagonalise the mass matrix by adopting a simple but efficient mass lumping scheme based on the row-sum method [46]. Before using such a method herein, the consistent mass matrix presented in Eq. (17) is integrated using the usual Gauss quadrature technique that is also recommended by Duczek and Gravenkamp [46]. This successfully worked with the present formulation and ensured conservation of the total mass of the structure.

A MATLAB code was then developed to implement the entire formulation in a generalized form for simulating high frequency wave propagation and scattering in composite and sandwich beams with any arbitrary laminations having multiple delaminations. The code can take any number of GLL points for the SFE, however, the analysis of numerical examples presented in this study adopted eight GLL points based on an initial convergence study of the solution accuracy.

3. Model verification

3.1. Wave propagating in intact composite beams

3.1.1. Wave velocity estimations

The performance of the proposed model for predicting wave propagation within a multi-layered composite beam is first tested in terms of its group (C_g) and phase (C_p) velocities. The laminated beam is 500 mm long, and 2 mm thick and consists of eight layers with a ply orientation of [0/90/0/90]s. The Cycom® 970/T300 graphite-epoxy, used for each equal-thickness plies, has material properties along their principal material axis: $E_1 = 128.75$ GPa, $E_2 = E_3 = 8.35$ GPa, $G_{12} = G_{13} = 4.47$ GPa, $G_{23} = 2.9$ GPa, $\nu_{12} = \nu_{13} = 0.33$, $\nu_{23} = 0.44$, $\rho = 1517$ kg/m^3.

To investigate both asymmetrical (A_0) and symmetrical (S_0) modes of guided waves, the beam is excited with a concentrated impulsive force $F(t)$ applied at its left end in the transverse and axial directions, respectively, as shown in Fig. 4. The force $F(t)$ is given in the form of a five-cycle Hann windowed tone burst pulse signal [47] with an amplitude of 1.0 N, which is kept unchanged in all cases as well as other examples. The beam is simulated using the proposed higher order beam model (HOSLM) where eight sub-laminates are used for simulating an eight layered beam to achieve high precision. From the time history analysis of the beam, the signals for its

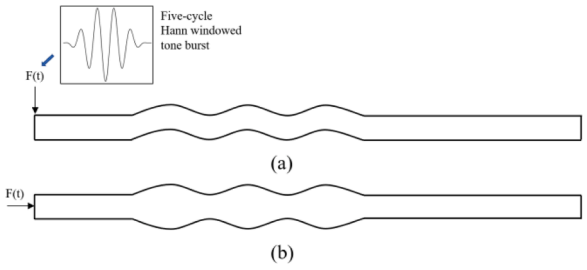

Fig. 4. (a) A_0 and (b) S_0 modes of guided waves.

response are captured at five locations/points along the beam length with an interval of 2.0 mm. With these signals (time-varying displacement), the group velocity is calculated as $C_g(f) = \frac{\Delta x}{\Delta T}$ where Δx is the distance between two adjacent points (2.0 mm in this case) and ΔT is the time needed by a wave to reach from one point to the next point i.e., a travelling distance of Δx. The calculation is repeated taking four different pairs of points from these five points, which show very little difference between their values, and these are averaged before reported in Fig. 5. In a similar manner, the phase velocity is calculated as $C_p = \frac{2\pi f \Delta x}{\Delta \Phi}$ where $\Delta\Phi$ is the phase difference of the wave at two adjacent points and f is the frequency of the pulse [47] used to excite the beam.

The excitation frequency (f) is varied from 20 kHz to 200 kHz with an increment of 20 kHz and the group and phase velocities estimated for A_0 and S_0 modes of waves are presented in Fig. 5. For the validation of these results, the Dispersion Calculator (DC) (i.e. a calculation tool developed by German Aerospace Centre [48]) is used and results produced by DC are included in Fig. 5. It shows a close correlation between the results obtained by the proposed model and DC, which gives initial confidence in using the present model.

3.1.2. Capabilities and performance of model in low frequency range

The accuracy of the present model in simulating wave propagation within composite beams is first studied by comparing results with those generated by existing models. For this purpose, a four layer laminated composite beam (0/90/90/0) is analysed. The beam is 500 mm long and 2 mm thick. The material properties of each equal-thickness ply are: $E_1 = 127$ GPa, $E_2 = E_3 = 7.9$ GPa, $G_{12} = G_{13} = 3.4$ GPa, $G_{23} = 3.435$ GPa, $\nu_{12} = \nu_{13} = 0.275$, $\nu_{23} = 0.15$, $\rho = 1578$ kg/m^3. The beam is excited by a 100 kHz pulse with five cycles at the beam's left end to generate the A_0 mode of guided wave. The present model with four sub-laminate is used to simulate the wave propagation. The deflection results are obtained on the top surface of the beam along the axial axis, and beam deflections against positions along beam axis when the propagation time (t_p) equal 200μs is plotted in Fig. 6. The same problem was also solved by Barouni and Saravanos [49] using a LW theory based model, and Rekatsinas et al. [50] using single layer based HSDT and FSDT models. Results produced by Those models are also shown in Fig. 6. The figure shows that the response predicted by the FSDT based model has obvious deviation compared to the LWT based model. Although the HSDT based model provides encouraging results, the right-half part of the signal still shows significant deviations. The present model also assumes a higher order variation through-thickness displacements, but it has capability of sub-lamination modelling which can improve modelling accuracy. It can be observed from Fig. 6 that the results produced by the present model match well with the benchmark results generated by the LWT based model. This is because that the present model performs like a typical LWT model when every physical layer is simulated by one sub-laminate. However, the present model can achieve higher computational efficiency than a typical LWT model by choosing an appropriate sublamination scheme, which will be investigated in the rest part of this section.

The sub-lamination capability of the proposed higher order beam model provides flexibility in balancing solution accuracy and computational efficiency. In order to assess this, different sub-lamination schemes of the model are used to simulate the laminated composite beam used in Section 3.1.1 by taking a specific case of the excitation (transverse impulsive force with 100 kHz excitation frequency) to produce A_0 mode of guided wave. A sub-lamination scheme is designated as SLS-n where n is the number of sub-laminates used for the whole laminate. In this case, four sub-lamination schemes are used, which are (i) SLS-1 (all 8 layers of the beam are accommodated by 1sub-laminate), (ii) SLS-2 (2 sub-laminates, each accommodated 4 layers; sub-laminate 1: 0/90/0/90, sub-laminate 2: 90/0/90/0), (iii) SLS-4 (4 sub-laminates, each accommodated 2 layers), and (iv) SLS-8 (8 sub-laminates, each accommodated 1 layer i.e., equivalent to a layer-wise model). The time-history for the transverse displacement (w) at the mid-span of the beam captured at its top surface is plotted in Fig. 7 that includes incident as well as reflected waves from the other end.

For verification of these results, a detailed 2D FE modelling-based simulation of the beam is undertaken using a reliable commercial FE code (ABAQUS/Explicit). The detailed model used 4-node rectangular plane stress elements (CPE4R), where the aspect (length-to-depth) ratio of elements is restricted to 2 to avoid any numerical disturbance. Two adjunct layers in thickness direction are connected by using 'tie constraint' in the intact region, and it is not applied in the delaminated region to simulate the delamination. For the

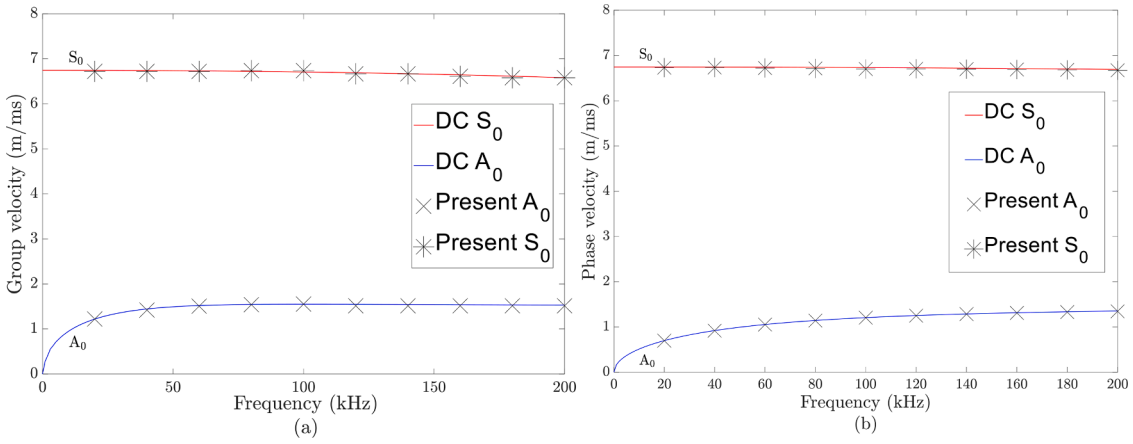

Fig. 5. Variation of (a) group velocity and (b) phase velocity with respect to excitation frequency (DC: dispersion calculator [48]).

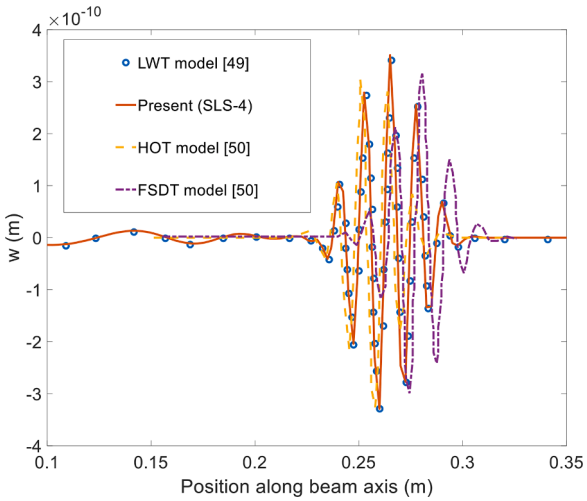

Fig. 6. Deflection response of beam's top surface along the beam axis for $t_p = 200\mu s$.

scenario that effect of contact is considered, 'surface to surface hard contact' is used in the delaminated region. Those procedure is consistently followed in the following examples. The strategy for validating results using detailed FE modelling is also employed in other examples when there are no suitable results available in the literature. In addition, a FSDT-based equivalent single layer SFE model [27] (implemented in a separate MATLAB code) is also used to solve the same problem. The results produced by these two modelling strategies are included in Fig. 7. It shows that the FSDT-based model performed worst considering the detailed FE modelling-based results as a reference. The FOSD-based model underestimated the wave amplitude and group velocity, which are more severe in the case of reflected waves. Compared to the FOSD-based model, the proposed model, even with the single sub-lamination scheme (SLS-1), has shown encouraging results in terms of a close prediction for the wave amplitude while the group velocity is slightly overestimated. The prediction of the proposed model is improved with the increase of sub-lamination numbers, because it helped to capture strain discontinuity (including transverse normal strain) at the interfaces between adjacent sub-laminates. It is interesting to observe that the improvement from SLS-1 to SLS-2 is not significant although it is significant from SLS-2 to SLS-4 while improvement from SLS-4 to SLS-8 is again insignificant. It is to be noted that SLS-4 and SLS-8 predicted results very close to the reference results. Thus, considering the computationally efficient of simulation, SLS-1 and SLS-4 are preferred options for this problem depending on the desired level of accuracy.

The same beam problem is used to study the computational efficiency of the proposed model and compared with that of the detailed FE modelling using ABAQUS (explicit). For this purpose, the number of degrees of freedom (DOF) needed to achieve a converged solution as well as the computing time for that solution is taken as the basis. Since it has been found above that SLS-4 sublamination scheme is a preferred option, it is used for the convergence study with respect to element size/number for discretisation along beam length. The convergence is also dependant on the size of the time step, which is automatically adjusted by ABAQUS using its in-build algorithm while a standard recommendation [18] ($\Delta t \leq 2/\omega_{max}$, where ω_{max} is the highest frequency of the structure) is followed for the proposed model. It has been found that the reflected wave needed finer meshing i.e., more elements to achieve converged results compared to the incident wave. The reflected wave predicted by these two modelling techniques using different mesh refinements is presented in Fig. 8, which shows that the proposed model needed a minimum of 5258 DOF (see Figure(a)) while the detailed FE model needed a minimum of 68,034 DOF (see Figure(b)). The simulations are conducted using the same computer (HP-Z2-G4 workstation, Intel i7–9700 CPU, 32GB RAM) for the proposed model and the detailed FE model. The minimum number of DOF and computing time needed by both modelling techniques are presented in Table 1, which clearly shows a significant reduction of computing time (87%) and memory (92%) by the proposed model. The table also included the case of SLS-1 of the proposed model that provided a further reduction of computation demand that may be appealing if not aiming for the highest precision.

Though the present study used explicit time integration for better computational efficiency, the proposed formulation was initially implemented within an implicit time integration-based scheme (Newmark method). In order to confirm that the solution accuracy was not compromised using the explicit time integration scheme, the same beam problem was analysed with the present model (SLS-4) with the implicit time integration scheme (with populated consistent mass matrix) where the same meshing was used. The results produced by both time integration schemes are presented in Fig. 9, which shows a very close agreement between them. However, the simulation based on implicit time integration has taken more than 5 times computing time using the same computer.

3.1.3. Capabilities and performance of model in high frequency range

The performance of the proposed model for capturing higher frequency waves is studied in this section. For this purpose, the same laminated composite beam studied in Section 3.1.2 is used however the beam length is reduced to 200 mm. Also, the excitation frequency is increased to generate waves in the structure that can have higher modes, unlike the previous section where the generated waves had fundamental mode only. To estimate the range of excitation frequency for this structure for this purpose, DC is used to create

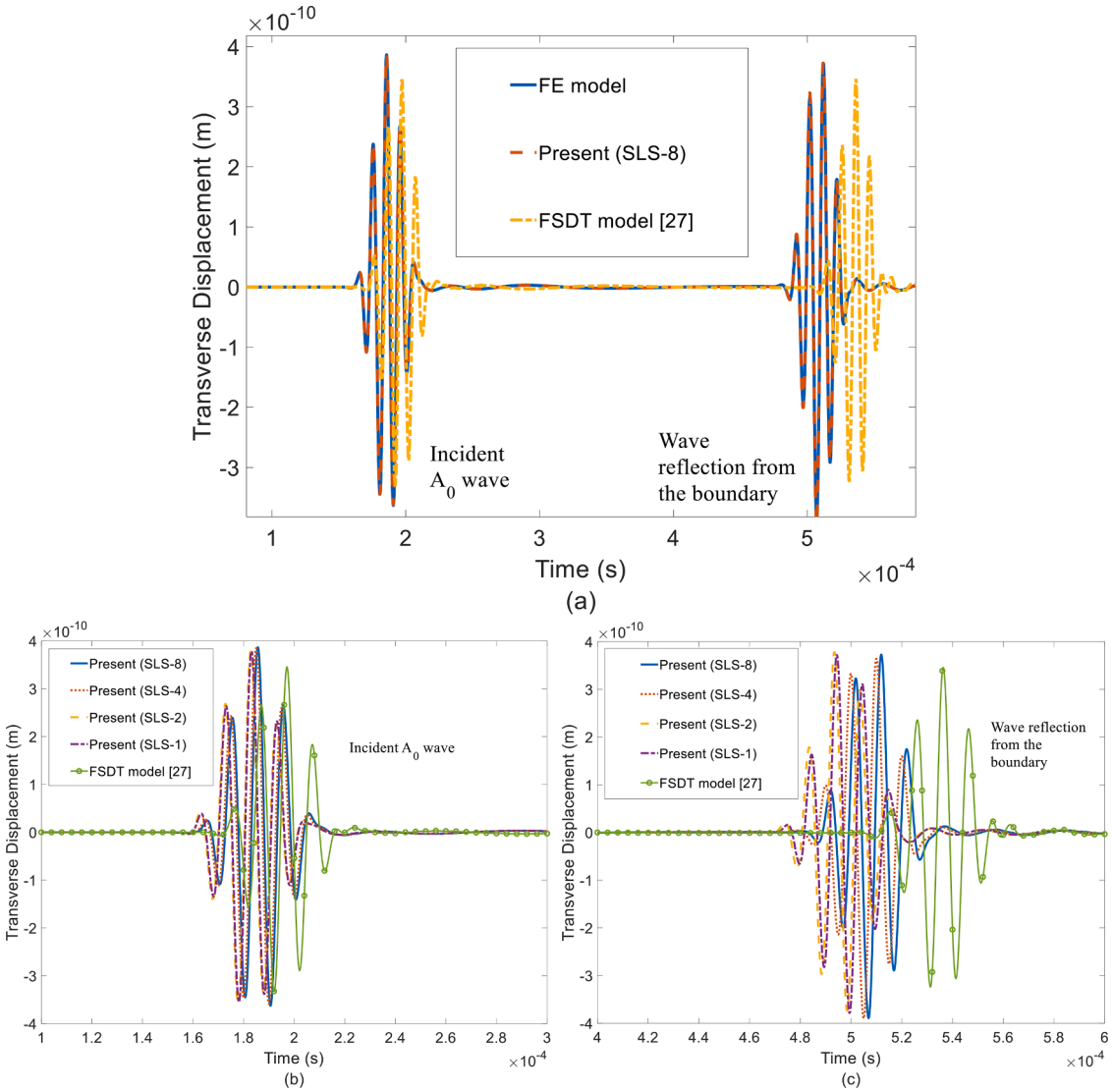

Fig. 7. Signal for beam mid-span (top surface) transverse displacement: (a) predicted by the present model (SLS-8), 2D detailed model, and FSDT based mode; (b) incident wave, and (c) reflected wave from beam end predicted by the present model with different sublamination schemes and FSDT based mode.

dispersion curves of waves produced in the beam, which are presented as a variation of wavenumber with respect to the excitation frequency in Fig. 10. The figure shows that the next higher modes appear when the excitation frequency exceeds a cut-off frequency, which is around 400 kHz for the asymmetrical wave (A_1) and 650 kHz for the symmetrical wave (S_1) in this problem.

To generate the higher mode of asymmetrical wave (A_1) in the laminated composite beam, the proposed model is employed to analyse the beam under a transversely applied excitation F(t) with 600 kHz frequency at one of the beam ends. The time-varying response (transverse displacement *w*) is captured near the other end of the beam (top surface), which is presented in Fig. 11. It is noted that the wave possesses both low velocity fundamental mode (A_0) and higher mode (A_1) having higher velocity, which are clearly shown in Fig. 11 (A_1 arrived at same measuring place much earlier than A_0). In a similar manner, the symmetrical mode of waves is investigated although the results are not reported to avoid repetition. The analysis of the beam is conducted with three sublimation schemes (SLS-8, SLS-4, and SLS-2) of the present model where a convergence study in terms of element size is made to have a stable result. The result (Fig. 11) shows that the performance of SLS-4 and SLS-8 is very close, as in the previous case while the performance of SLS-2 is deteriorated further compared to the low frequency case. The proposed model is therefore capable of capturing all modes (fundamental and high modes) accurately unlike some existing models [30].

To identify the different wave modes for an unknown problem having test data, the time-domain response can be transformed into the frequency domain where the separation of different wave modes can result in clearer visualisation. For this purpose, a two-dimensional Fourier transform (2D FT) technique [51] is used that requires time-domain responses at a number of equally spaced

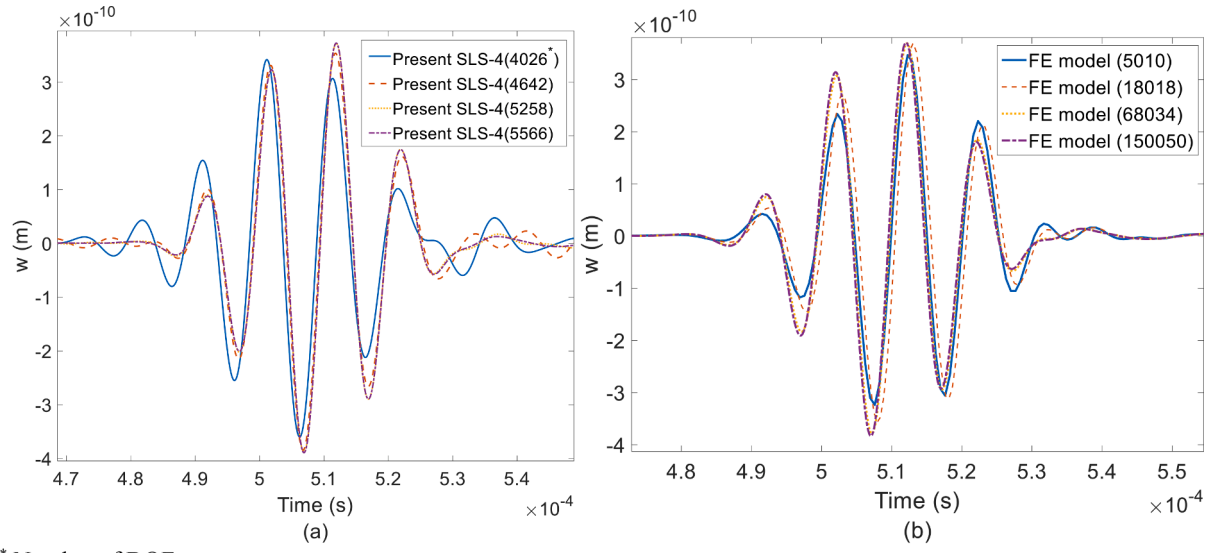

Fig. 8. Convergence study for the same response (Fig. 7c)) using the (a) present model (SLS-4), (b) detailed FE model.

Table 1
Computational efficiency of present model with reference to detailed FE model in low frequency range.

	Detailed FE model	Present model (SLS-4)	Present model (SLS-1)
Degrees of freedom (DOF)	68,034	5258 (92%*)	1673 (98%)
Computing time (*sec*)	3180	409 (87%)	34 (99%)

* % reduction compared to the detailed FE model.

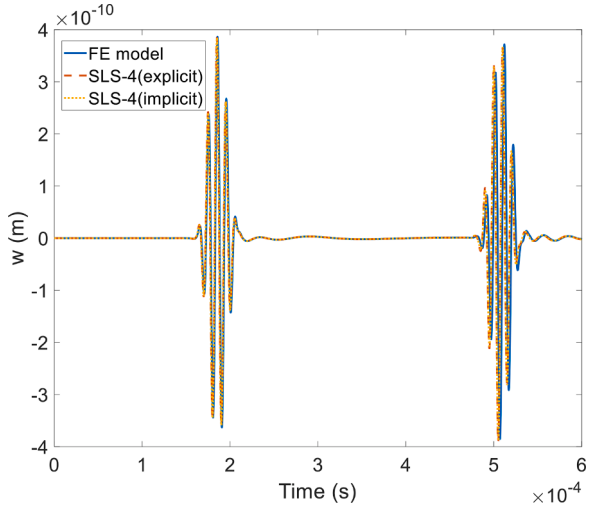

Fig. 9. Signal for beam mid-span (top surface) transverse displacement using present model (SLS-4) based on explicit and implicit time integrations.

measurement points along the direction of wave travel. The 2D FT produces the frequency-wavenumber spectrum that helps to easily separate the multiple modes for visualisation purposes. The time-domain responses obtained from the present analysis (SLS-4) are measured at 21 points aligned along the beam length (top surface) with a spacing of 1.0 mm, which at a distance of 50.0 mm and ended at 70.0 mm from the beam end subjected to excitation. The frequency-wavenumber spectrum produced by the 2D FT is presented in Fig. 12, which is also superposed with the dispersion curves (Fig. 10) obtained using DC. Two densified regions appear in Fig. 12a, which clearly shows that the central frequency of the wave that is equal to the excitation frequency is around 600 kHz. There are also two wave modes, which are A_0 and A_1 in this case. This is similarly observed in Fig. 12b for the symmetrical mode of waves where the

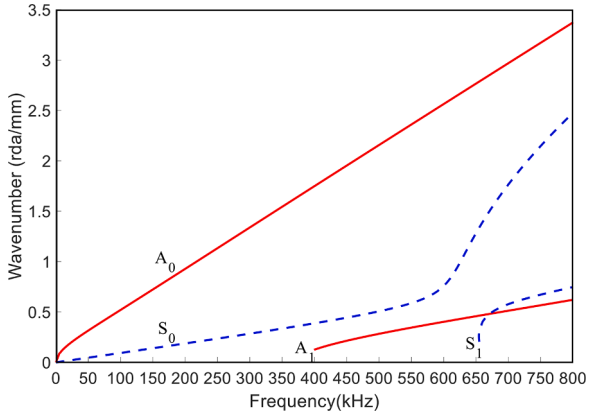

Fig. 10. Dispersion curve for the laminated composite beam (A_0 and S_0 - fundamental mode and A_1 and S_1 - next higher modes).

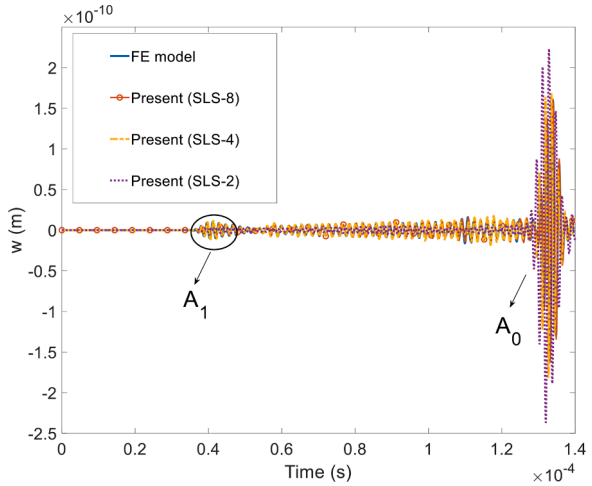

Fig. 11. Time-history responses of transverse displacement for 600 kHz asymmetrical guided wave predicted by different models.

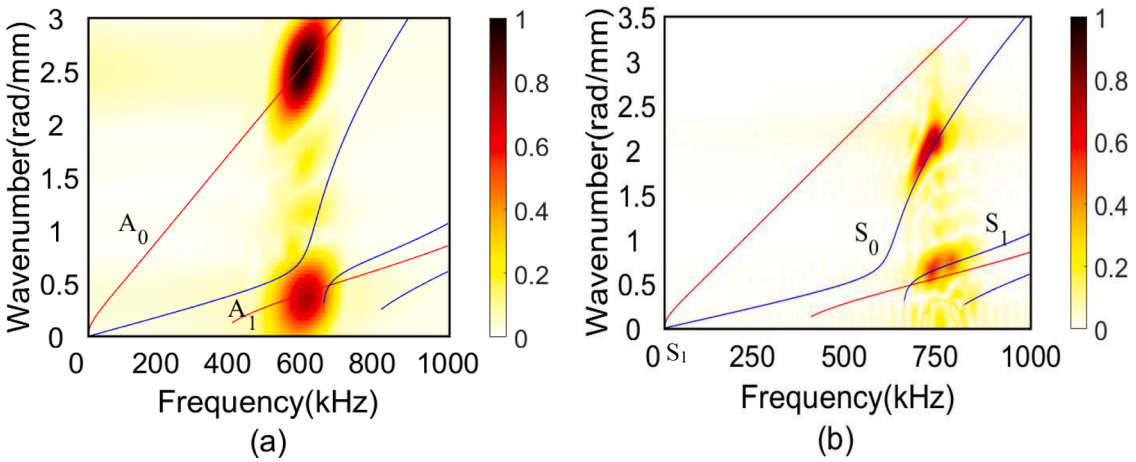

Fig. 12. Frequency-wavenumber spectrum for (a) asymmetrical, (b) symmetrical modes of guided wave in laminated composite beam.

central frequency of the wave is found to be 750 kHz, which is actually given as the input for the excitation frequency in conducting the time history analysis.

To assess the computational efficiency of the present model in the high frequency range, similar to that presented in Section 3.1.2 for low frequency, the scenario for the asymmetrical mode of waves produced with the excitation frequency of 600 kHz is chosen to present the results in terms of computing time and number of unknowns (DOF). These are shown in Table 2 and compared with those needed by the detailed FE model. The table shows a similar level of computational efficiency in the high frequency range. For the present problem, the number of unknowns is reduced by 98% and it is 91% for the computing time.

3.1.4. Wave attenuation due to damping

Damping is one of the main factors causing wave attenuation in addition to any dispersive actions. A laminated composite (0/90/0) beam is used herein to investigate the performance of the present model in simulating attenuation of guided waves within the beam due to damping. The beam consists of three equal-thickness glass fibre reinforced epoxy layers, and their material properties along the principal material axis are: $E_1 = 44.68$ GPa, $E_2 = E_3 = 6.90$ GPa, $\nu_{13} = 0.28$, $\nu_{23} = 0.355$, G_{13}=2.54 GPa, $\rho = 1990$ kg/m^3. The beam is 300 mm long and 0.99 mm thick (each layer 0.33 mm thick). The beam is excited with a similar pulse having seven-cycle and 200 kHz of excitation frequency to produce A_0 mode of guided wave in the beam, and the wave response is captured at 9 points along the beam length (top surface) at an interval of 10 mm where the first measurement point is 5 mm away from the beam end subjected to the excitation. This problem was studied by Ramadas et al. [52] using a detailed FE model to analyse the beam utilising Rayleigh's damping model. The same damping parameters ($a_0 = 13.536\ rad/s$ and $a_1 = 8.571 \times 10^{-9} s/rad$) provided by them are used in the present analysis. The wave amplitudes predicted by the present model (SLS-3) at each measurement point are normalised to that at the first measurement point and plotted in Fig. 13. The published results [52] are also presented in Fig. 13 for validation. The figure shows satisfactory agreement between the reference results and those produced by the present model.

3.2. Wave propagation in delaminated beams

3.2.1. Delaminated composite beam considering no effect of contact

To investigate the performance of the proposed mode to simulate wave propagation in delaminated composite beams, the present model is first used to analyse a three-layer glass/epoxy laminate containing a relatively larger asymmetrically located delamination (Fig. 14). The same material in Section 3.1.4 is used herein for each equal-thickness ply. The beam is excited with a 200 kHz pulse with seven-cycle to produce A_0 mode of guided wave in the beam by giving transverse load at the top and bottom surface of the beam end (Shown in Fig. 14). The response of deflection predicted by the present model using three sub-laminates (SLS-3) is obtained at 100 mm away (point A in Fig. 14) from the excitation point, and the result is shown in Fig. 15. The same problem is also solved by Ramadas et al. [53] using 2D detailed FE model, and the result is also plotted in Fig. 15. The figure shows high agreement between the results from literature [53] and those produced by the present model.

To further study the performance of the sublamination capability of the presented model, the eight-layered composite used in Section 3.1.1 (same geometry and materials) is adopted herein but a smaller 2.0 mm long delamination is incorporated between the 4th and 5th layers near the middle of the beam length as shown in Fig. 16. The beam is excited with the same five cycle pulse and an excitation frequency of 100 kHz is used to produce an A_0 mode of guided wave. Since the minimum number of sub-laminates required by the present model is 2 to model the laminated beam with one delamination, the sub-lamination schemes used are SLS-8, SLS-4 and SLS-2. The wave response predicted by the proposed model is captured at Points A and B (see Fig. 16) and presented in Fig. 17. Fig. 17a corresponding to point A shows the incidental wave followed by the reflected wave produced by the wave interaction with the delamination (a portion of the wave) while Fig. 17b (point B) shows the transmitted wave (reaming portion of the wave). To validate these results, the problem is also solved via the detailed FE model and the results obtained are included in Fig. 17. The figure shows that both sub-lamination schemes SLS-8 and SLS-4 of the present model performed in a similar manner to the detailed FE model. Although the present model with SLS-2 slightly overestimated the velocity of the reflected and transmitted wave, it could be a better option for higher computational efficiency if that high prediction is not required.

Wave propagation in a laminated composite beam with multiple de-laminations is now investigated. The same 8 layered compose beam is considered although two de-laminations at two different locations and planes as shown in Fig. 18 is analysed for this purpose. The first delamination (d_1) having a length of 4.0 mm is located at the interface between the 4th and 5th layers near the middle part of the beam length. The second delamination (d_2) having a length of 2.0 mm is located between the 6th and 7th near the quarter part of the beam length close to the end that is subjected to excitation. To accommodate two delaminations, at least 3 sub-laminates are required by the present model. Thus, the three sub-laminate schemes used for modelling the beam are: (i) SLS-3 (sub-laminate 1: 0/90/0/90 at top, sub-laminate 2, (ii) 90/0 at middle, sub-laminate 3: 90/0 at bottom), and (iii) SLS-4 and SLS-8. With the same excitation at the right end of the beam, the wave (A_0) response for w predicated by the model (SLS-3, SLS-4 and SLS-8) at points A, B and C (see

Table 2
Computational efficiency of present model compared to detailed FE model in high frequency range.

	Detailed FE model	Present (SLS-4)
Degree of freedom (DOF)	648,162	10,802 (98%*)
Analysis time (*sec*)	12,925	1137 (91%)

* % reduction compared to the detailed FE model.

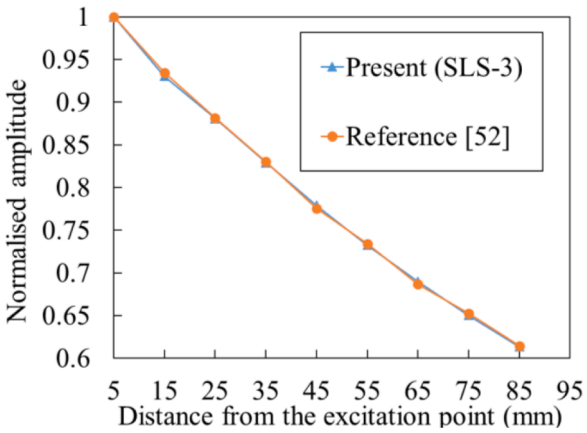

Fig. 13. Reduction of wave (A_0) amplitude along beam axis showing wave attenuation in composite beam due to damping.

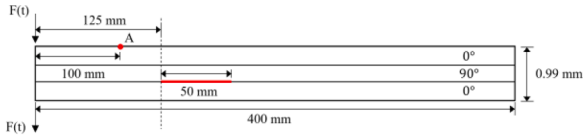

Fig. 14. Composite laminate with an asymmetrically located delamination.

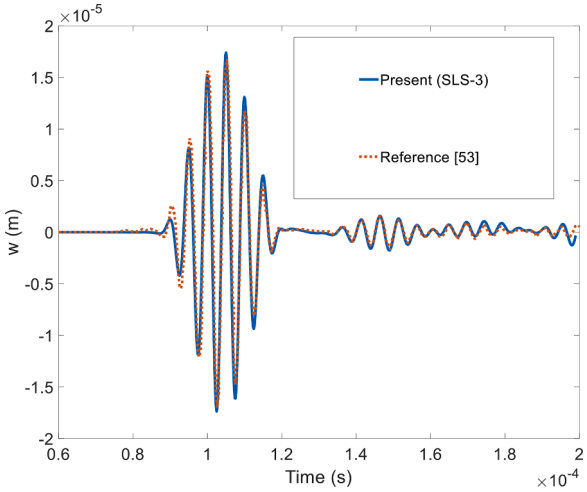

Fig. 15. Time history for wave responses (w) of composite beam with single delamination captured at locations A (Fig. 14).

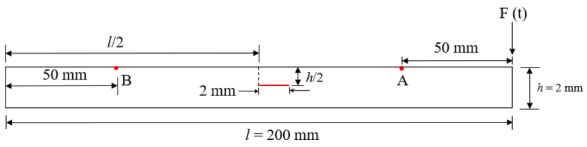

Fig. 16. Laminated composite beam with single mid-plane delamination.

Fig. 18) is plotted in Fig. 19a, 19b, and 19c, respectively.

Compared to the incident wave (see Fig. 19a, point A), the amplitude of the transmitted wave obtained after passing through the delamination d_2 (see Fig. 19b, point B) became bit lower, which is then further reduced a bit when the wave transmitted through another delamination d_1 (see Fig. 19c, point C). This behaviour is expected since the wave is likely to lose a portion of its energy when it interacts with a delamination. The wave started travelling from the right end to the left end and the incidental wave having its full

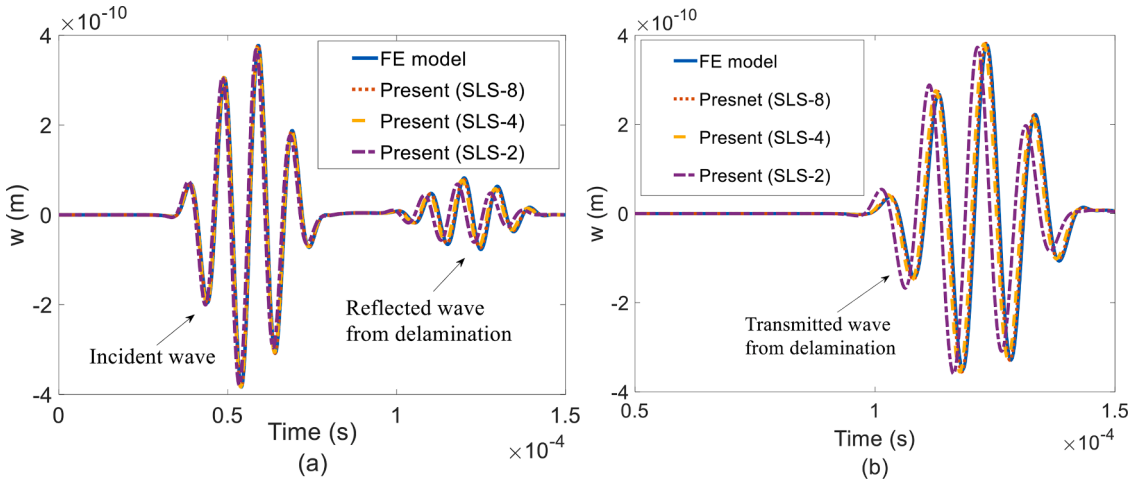

Fig. 17. Time history for wave responses (w) of composite beam with single delamination captured at (a) locations A, (b) location B (see Fig. 16).

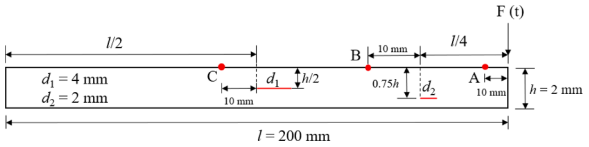

Fig. 18. Laminated composite beam having two de-laminations at different interfacial planes and locations.

energy is captured at point A that appeared as the first part of the plot shown in Fig. 19a. The wave is moved forward (towards left) and interacted with the delamination d_2 where a part of the wave energy moved forward as transmitted wave that is captured at B (first part of the plot in Fig. 19b) while the reaming energy moved backward as reflected wave that is captured at A (second part of the plot in Fig. 19a). The transmitted wave from d_2 then moved forward and interacted with delamination d_1 where a part of this wave is transmitted that is captured at C (Fig. 19c) while the remaining part of this wave is reflected that is captured at B (last part of the plot in Fig. 19b). The reflected wave from d_1 is again interacted with the de-lamination d_2 and its transmitted part is captured at A (last part of the plot in Fig. 19a). This part is likely to be combined with the initially reflected wave form d_2 that reflected from the right end.

The beam is similarly analysed with the detailed FE model and the results obtained are included in Fig. 19. The figure shows that the present model with minimum number of sub-laminates (SLS-3) provided a good prediction for wave amplitude, although the wave velocity was slightly overestimated. This deviation, however, increased gradually with the increase of wave travel time/distance. Unless a prolonged wave propagation is simulated, model SLS-3 can be recommended for such problems owing to better computational efficiency.

3.2.2. Delaminated sandwich beam considering no effect of contact

The performance of the proposed model in simulating wave propagation within a delaminated sandwich beam is studied in this section. For this purpose, a sandwich beam (0/90/C/90/0) with a thick core layer (10 mm thick) sandwiched between two symmetrically placed identical laminated face sheets (each ply 0.5 mm thick) is used. This beam (1000 mm long and 12 mm thick, Fig. 20) has a delamination (10 mm long) at the interface between the core and top face sheet near the mid-length of the beam. The material properties of the laminated sheets (graphite-epoxy) are the same as those used in Section 3.1.1 while the core material properties core are: $E_1 = E_2 = 0.08{,}040$ GPa, $E_3 = 1.005$ GPa, $G_{12} = 0.03{,}220$ GPa, $G_{13} = G_{23} = 0.1206$ GPa, $\nu_{12} = 0.25$, $\nu_{13} = \nu_{23} = 0.02$, $\rho = 64\ kg/m^3$.

The beam is excited with the same five-cycle pulse (see Section 3.1.1) at its right end to generate an A_0 mode of guided wave. After interaction of the wave with the delamination, the wave response is captured at point A (see Fig. 20) as well as the loaded point in order to respectively capture the transmitted and reflected waves. To assess the range of excitation frequency needed for this purpose, the dispersion curve of the sandwich beam is first produced by using the DC, which are plotted in Fig. 21. The figure shows that the higher order wave mode (A_1) is generated along with the fundamental mode (A_0) when the wave frequency exceeds 20 kHz. To avoid the appearance of the A_1 mode of wave that may make the wave response signal too noisy to hinder an easy damage detection, an excitation frequency of 15 kHz is selected. For the analysis of the beam with the present model, two sub-laminate schemes (SLS-5 and SLS-3) are used to accommodate the delamination. The time-history for the wave responses (w) predicted by these models are plotted in Fig. 22, which shows that model SLS-3 is adequate to accurately predict reflected and transmitted waves for a thick sandwich beam.

The computational efficiency of the present model for simulating this beam problem is also studied. The computational demands required by the present model (SLS-3) and the detailed FE model to achieve stable converged results are presented in Table 3. This shows that the present model can save 97% of unknown variables and 90% of analysis time compared to the detailed model in

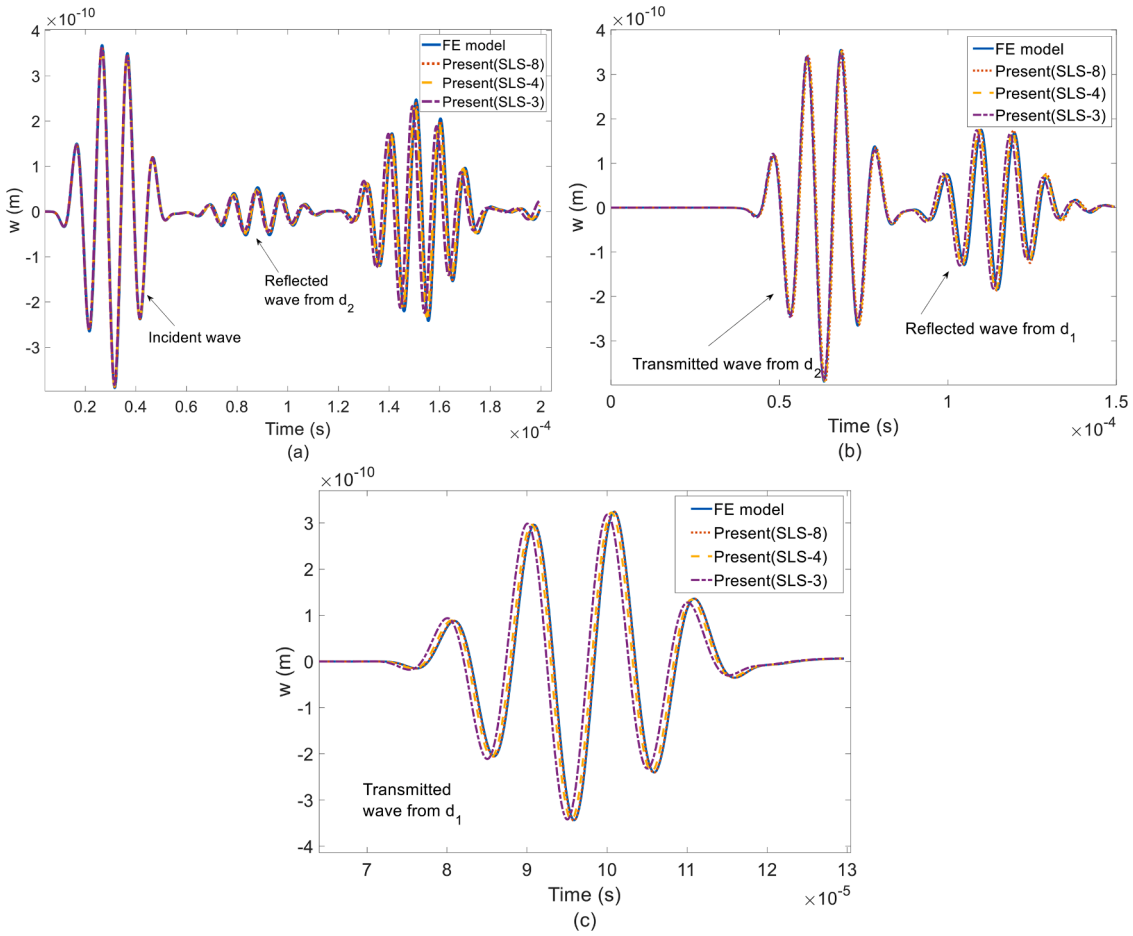

Fig. 19. Time-history for wave responses (w) of composite beam with multiple de-laminations captured at (a) location A, (b) location B, (c) location C (see Fig. 18).

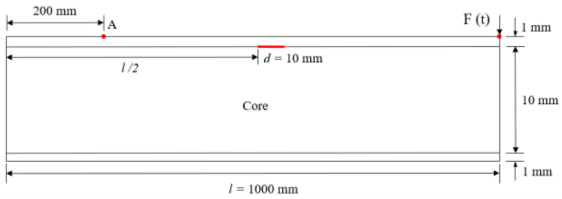

Fig. 20. Sandwich beam containing delamination.

simulating wave propagation within the delaminated sandwich beam.

3.2.3. Contact nonlinearity effect on wave propagation in delaminated composite beam

Contact is one of the nonlinear phenomena observed in the propagation of guided wave in a structure when the wave interacts with a damage such as delamination where the contact between damaged surfaces is activated or deactivated depending on the nature of loading that leads to generation of higher harmonics. This is due to clapping of the two surfaces of a delamination in mode I or closing-opening mode of deformation. This nonlinear behaviour has drawn much attention since it is more sensitive to small damage [54]. As mentioned in Section 2, the present model incorporated a penalty-based technique to simulate contact behaviour in the delaminated region. To investigate the performance of the present model in capturing contact nonlinearity, the same problem used in Section 3.2.1 is considered herein for this purpose. The position of the delamination is also moved up from the mid-plane (interface between 4th and 5th layers) of the 8 layered beam to the interface between the 2nd and 3rd layers. This is done on the basis of an existing study [55] where it is stated that the placement of a delamination at the mid-plane of a symmetrical laminated beam is likely to produce an insignificant higher harmonic that may be hard to recognise.

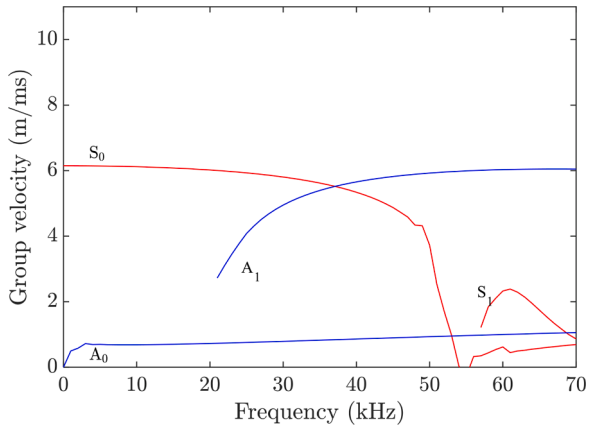

Fig. 21. Dispersion curves (group velocity) of delaminated sandwich beam.

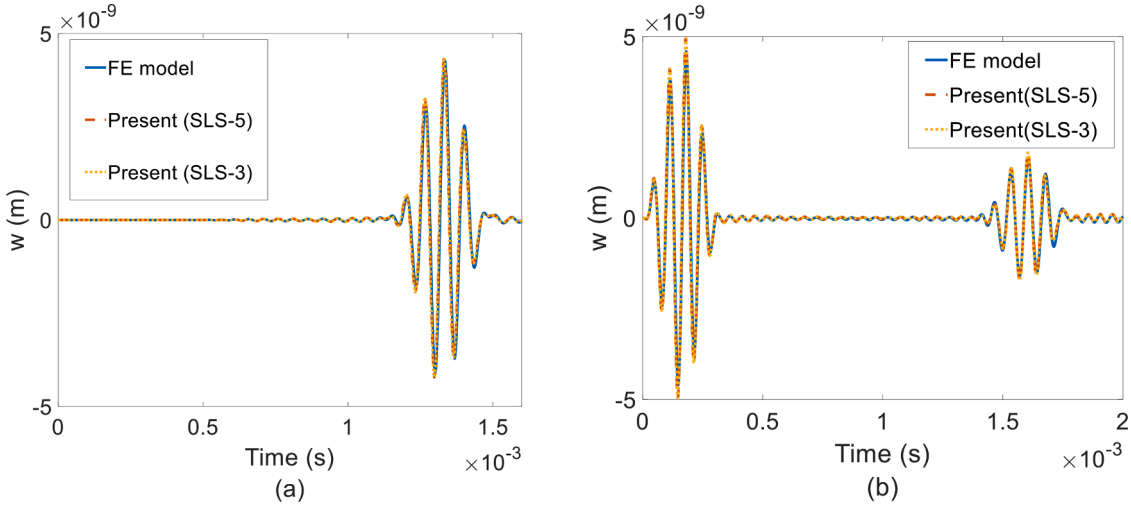

Fig. 22. Time-history of wave responses of delaminated sandwich beam (Fig. 20) at (a) point A, (b) excitation point.

Table 3
Computational efficiency of proposed model for simulating wave (A_0) propagation within delaminated sandwich beam.

	Detailed FE model	Present (SLS-3)
Degrees of freedom (DOF)	175,666	5979 (97%*)
Computing time (*sec*)	41,934	4133 (90%)

* % reduction compared to the detailed FE model.

The present model (SLS-4) is used to reanalyse the beam here with and without using the contact model. In this case, the time history for the wave response (w) predicted by the model for these two cases is captured at a point (beam top surface) 50 mm away from the excitation point. As it can be difficult to detect the influence of higher harmonics in the time domain, the time history-based wave response data is converted to the frequency domain using a fast Fourier transform (FFT) technique. Before performing the FFT, the wave response (time domain) is processed by subtracting with corresponding wave response of the same beam with no damage (baseline subtraction technique) to retain only the damage contribution. The results obtained for the two cases with and without contact are presented in Fig. 23 along with those produced by the detailed FE model with contact simulated using the surface-to-surface based contact algorithm of ABAQUS. The figure shows the higher harmonics in the form of a hump around 200 kHz (2 times of the excitation frequency), which is observed only for simulations exhibiting the contact phenomenon.

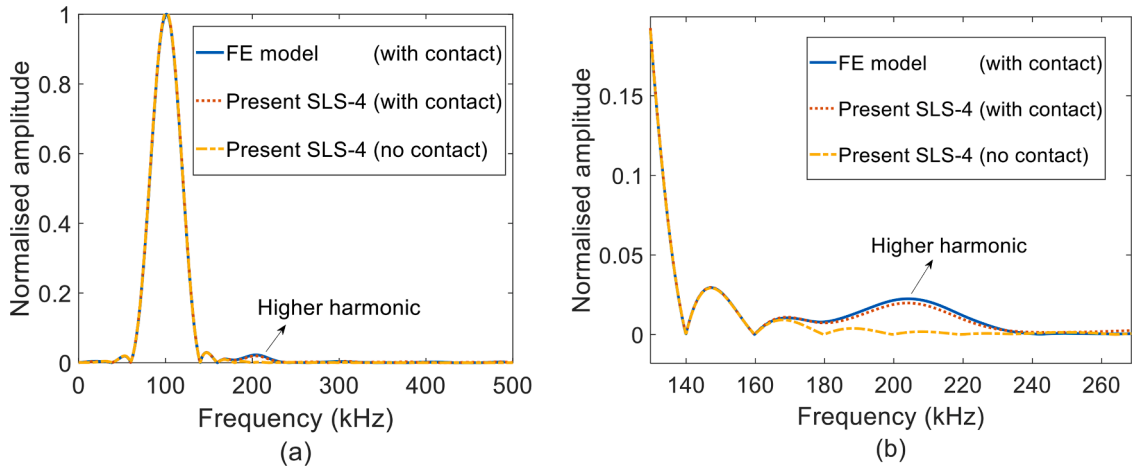

Fig. 23. (a) Wave response in frequency-domain of delaminated beam simulated with and without contact, (b) magnified view of higher harmonics.

4. Influence of delamination size and location on wave response of sandwich beam

The performance (accuracy and computational efficiency) of the proposed model in simulating the propagation of a guided wave within composite/sandwich beams with/without delamination has been successfully verified in the previous section. Based on this confidence, the model is now used to investigate the influence of delamination size and location on the wave responses of a sandwich beam (Fig. 24). The 1000.0 mm long beam (0/90/0/90/C/90/0/90/0) has two symmetrically placed identical laminated face sheets each having four layers. The material properties for the core (10 mm thick) and each ply (0.25 mm thick) are the same as those utilised in Section 3.2.2.

The location of the delamination (see Fig. 24) is varied by changing its interfacial position of the upper laminate face sheet and with no change in horizontal placement. This has resulted in four damage case scenarios, which are defined as (i) D1 (interface between 1st ply, i.e., topmost ply, and 2nd ply), (ii) D2 (interface between 2nd ply and 3rd ply), (iii) D3 (interface between 3rd ply and 4th ply), and (iv) D4 (interface between 4th ply and core layer). The delamination length is variated from 5 mm to 30 mm with an increment of 5 mm. This results in 6 scenarios, and all these scenarios are investigated under each of the damage cases (D1-D4).

To estimate the range of excitation frequency, the dispersion curves of the beam are first determined using DC which and plotted as wavelength versus frequency in Fig. 25. In order to have a clearer wave response for easy damage detection, the excitation frequency should be chosen so that the appearance of higher modes (A_1 or S_1) can be eliminated. Amongst the two options for the fundamental modes, the asymmetrical mode (A_0) is preferable than the symmetrical mode (S_0) since the wavelength for A_0 is smaller (see Fig. 25) compared to S_0, which is beneficial for detecting smaller size defects. Based on this observation, the beam is excited transversely at its right end (see Fig. 24) using a five cycle pulse having a frequency of 15 kHz to generate an A_0 mode of the wave within the beam. The reflected and transmitted wave generated after interaction of the incident wave with the delamination is captured at Points A and B (see Fig. 24), respectively. Although there are many damage scenarios, the influence of a small damage is insignificant on dispersion curves.

Since the number of damage scenarios/cases is large, the transmitted and reflected wave response are presented in the form of their amplitudes only. These are again estimated from the wave response in the time domain as well as the frequency domain following the process stated in Section 3.2.3. As the wave response in the time domain can only demonstrate the primary component of the wave propagating with the beam effectively, it can be used to get a global scenario of wave propagation. But it is not effective to get a local picture in the form of higher harmonics (high frequency with low amplitude) produced by a localised damage through some action such as clapping that needs a frequency domain based estimation. Thus it is important to consider the effect of contact in the frequency domain based analysis while it is not key for time domain based analysis.

Fig. 26 presents variations of reflected and transmitted wave amplitudes obtained from time domain data with respect to the delamination length for the four damage locations (D1-D4). In all cases, the wave amplitudes are normalized with their incident wave

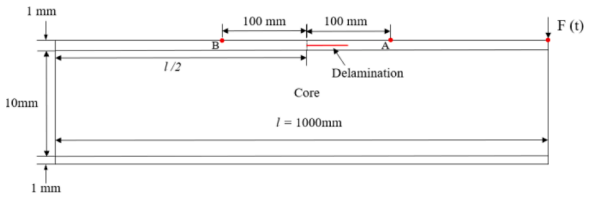

Fig. 24. Laminated sandwich beam (0/90/0/90/C/90/0/90/0) with varied length and location of delamination.

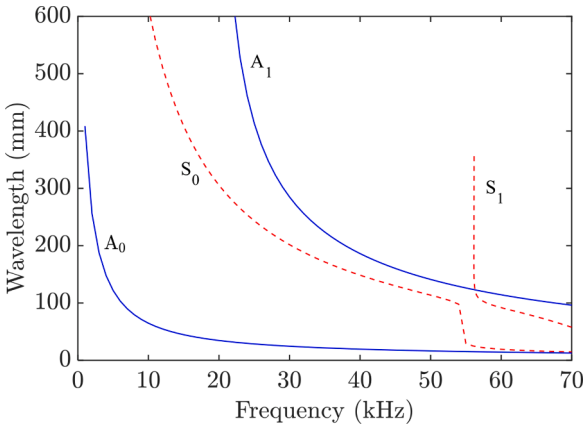

Fig. 25. Dispersion curves of nine-layered sandwich beam (Fig. 24).

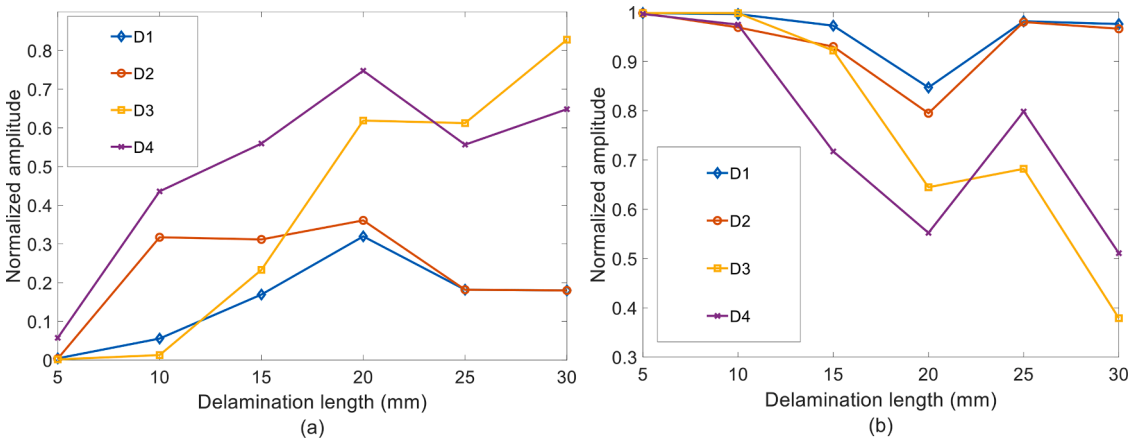

Fig. 26. Variations of wave amplitudes for the (a) reflected and (b) transmitted obtained from time domain data with respect to the delamination length and locations.

amplitudes. Fig. 26a shows that the reflected wave amplitudes for D2 and D4 are higher than D1 and D3 when the delamination length is less than 15 mm. When the delamination length increases beyond 15 mm, the amplitudes for D3 and D4 are found to be much higher than other damage cases while the maximum amplitude occurs for D3 for 30 mm long delamination. Fig. 26b presents the amplitudes of the transmitted waves, which demonstrate a decreasing trend initially with the increase of delamination size. It is also found to have an opposite trend when the delamination size exceeds 20 mm to 25 mm. In this case, the minimum amplitude occurs for D3 when delamination is 30 mm long and this same damage scenario provided the maximum amplitude of the reflected wave.

Fig. 27 presents the variations of amplitude of higher harmonics with respect to the delamination length and damage locations (D1-D4) for the reflected wave (point A) and the transmitted wave (point B). These are obtained following the same frequency domain-based technique described in Section 3.2.3. As shown in Fig. 27a and b, the amplitude (D1 and D2) increased with increase of delamination length up to a certain limit and it is then decreasing dropped down gradually. Fig. 27c and d show that the amplitude for D3 and D4 increased with the delamination length with no steady reduction except some fluctuations. This indicates that the higher harmonic amplitude does not always increase with the delamination length since the behaviour is also affected by the delamination location. Moreover, the amplitude for the reflected wave is larger than the transmitted wave for all cases except in one case (D2). Thus the use of reflected wave which generally having a stronger signal should be preferable for damage detection through higher harmonics. In simulation of this phenomena, the model should have the provision of contact that will induce nonlinearity in the response leading to higher harmonics.

4. Conclusion

A higher order laminate model is developed within a spectral finite element (SFE) framework in this study to simulate the propagation of guided waves in delaminated composite and sandwich beams. The model has the capability of sub-lamination based modelling where each sub-laminate adopted a cubic variation of in-plane displacement and a quadratic variation of transverse

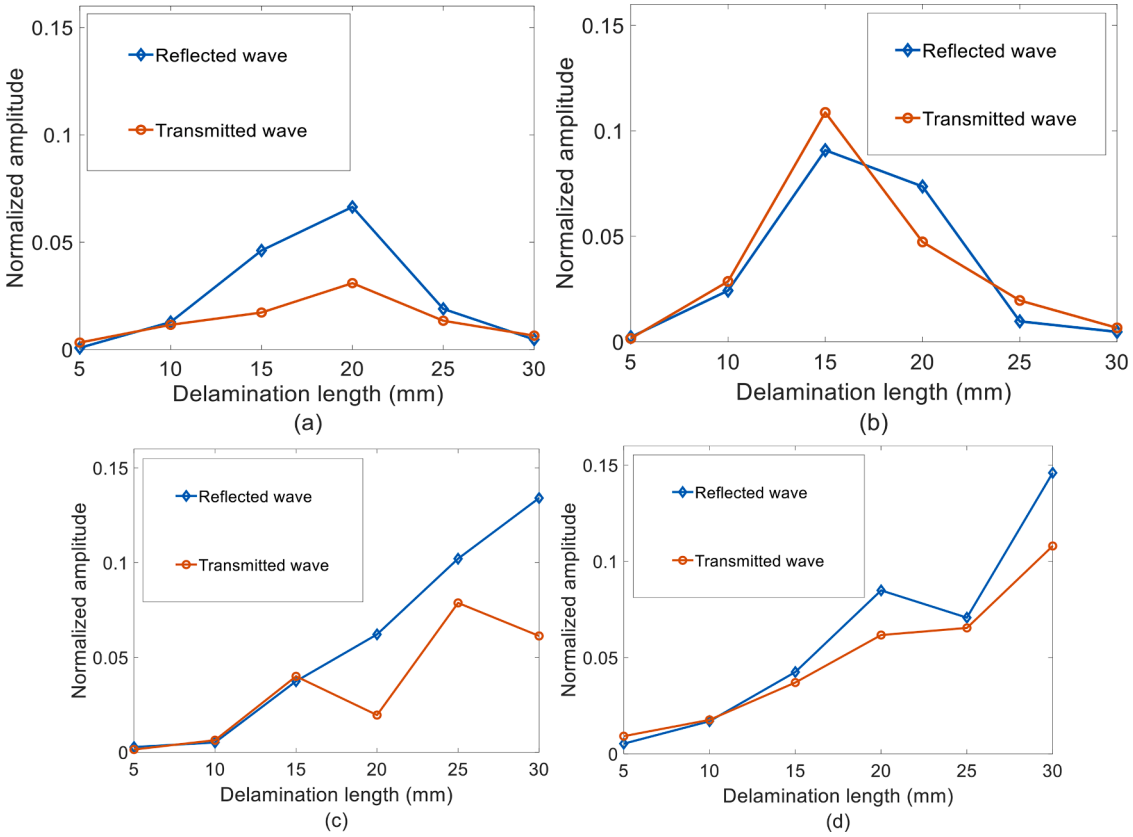

Fig. 27. Variations of higher harmonic amplitudes (processed data in frequency domain) with respect to delamination length and location: (a) D1, (b) D2, (c) D3, and (d) D4.

displacement through the thickness. These high order displacement formulations are expressed by unknown displacements at exterior (top and bottom) surface, which are beneficial for modelling multilayered structures accurately. This can be achieved by stacking several sub-laminates in the thickness direction and connecting them with their exterior surface nodal displacements directly without any additional treatment. In that case, delamination can be conveniently inserted between two adjunct sub-laminates, where the unknown displacements at their top and bottom surfaces are connected by high stiffness springs to simulate contact behaviour within the delamination. These springs are activated during delamination closing while deactivated during delamination opening. In order to achieve a higher computational efficiency, multiple layers having no delamination within these layers can be accommodated into one higher order sub-laminate with no significant loss of accuracy. Based on the proposed laminate model, a C° continuous SFE code is developed using MATLAB. The code is written in a general form so that it can accommodate any number of nodes within an element to achieve any level of accuracy. Similarly, the model can also cater for different levels of discretisation in the thickness direction by using a different number of sub-laminates. The model therefore has high flexibility to trade-off between accuracy and computational effort.

The performance of the proposed model is examined by simulating several numerical examples of wave propagation within composite and sandwich beams. Initially, wave velocities are calculated for different excitation frequencies. The model is then used to simulate wave propagation (in lower and higher frequency ranges) within intact composite beams. In addition, the model is utilised to simulate wave attenuation due to damping within an intact composite beam. The wave propagation within composite and sandwich beam with delaminations is then simulated using the model. These problems are used to test the ability of the model for capturing higher harmonics induced by a clapping mechanism within the delamination region. For the validation of our results, 2D detailed FE models are produced using a commercial FE code (ABAQUS) to solve the same problem. The results show that the proposed model can save more than 90% computing time and memory compared those needed by the commercial FE code with similar level of solution accuracy.

After successful validation, the proposed model is used to investigate the influence of delamination size and locations on the amplitude of responses for sandwich beams. The following observations are made from the time domain response:

- In general, the amplitude for the reflected wave exhibits an increasing trend with an increasing of delamination size while the transmitted wave has an opposite trend.

- The location of delamination has a prominent effect on the wave response amplitude. The amplitude of the wave reflected from the delamination is smaller in most of cases when the delamination is located at an interface away from the core while it is larger when the delamination is close to core layer.

Similarly, the following observations are made from the frequency domain response:

- The amplitude of the higher harmonics obtained from the reflected wave is higher than that obtained from the transmitted wave in most of cases.
- For both the transmitted and reflected waves, the amplitude of the higher harmonics exhibits a similar trend with change of delamination location and size. The amplitude is initially increased and then drops when the delamination size increases for the sandwich beam containing delamination away from the core, while this has a steady increasing trend when the delamination is located close to the core layer.

Data availability

Data used in this research can be available from the lead author (Yuan Feng, Email: yuan.feng525@gmail.com; yuan.feng@adelaide.edu.au) on request.

CRediT authorship contribution statement

Yuan Feng: Conceptualization, Formal analysis, Investigation, Methodology, Validation, Software, Writing – original draft. **Abdul Hamid Sheikh:** Conceptualization, Methodology, Validation, Supervision, Writing – review & editing. **Ching-Tai Ng:** Methodology, Supervision, Software, Writing – review & editing. **Scott T. Smith:** Methodology, Supervision, Writing – review & editing.

Declaration of Competing Interest

The authors declare that they have no known competing financial interests or personal relationships that could have appeared to influence the work reported in this paper.

Acknowledgments

Support provided by the Australian Research Council (ARC) via Discovery Grant DP220103665 is gratefully acknowledged.

References

[1] G.H. Staab, V. Pearson, Laminar Composites, 2nd edition. ed., Butterworth-Heinemann, Amsterdam, [Netherlands, 2015.
[2] V. Giurgiutiu, J. Bao, Embedded-ultrasonics structural radar for in situ structural health monitoring of thin-wall structures, Struct. Health Monit. 3 (2004) 121–140.
[3] J.B. Ihn, F.K. Chang, Pitch-catch active sensing methods in structural health monitoring for aircraft structures, Struct. Health Monit. 7 (2008) 5–19.
[4] M. Rucka, Experimental and numerical study on damage detection in an L-joint using guided wave propagation, J. Sound Vib. 329 (2010) 1760–1779.
[5] C.T. Ng, M. Veidt, Scattering of the fundamental anti-symmetric Lamb wave at delaminations in composite laminates, J. Acoust. Soc. Am. 129 (2011) 1288–1296.
[6] A. De Miguel, A. Pagani, E. Carrera, Higher-order structural theories for transient analysis of multi-mode Lamb waves with applications to damage detection, J. Sound Vib. 457 (2019) 139–155.
[7] M. Filippi, A. Pagani, E. Carrera, High-order finite beam elements for propagation analyses of arbitrary-shaped one-dimensional waveguides, Mech. Adv. Mater. Struct. 29 (2022) 1883–1891.
[8] H. Sohn, G. Park, J.R. Wait, N.P. Limback, C.R. Farrar, Wavelet-based active sensing for delamination detection in composite structures, Smart Mater. Struct. 13 (2003) 153.
[9] Z. Su, L. Ye, Y. Lu, Guided Lamb waves for identification of damage in composite structures: a review, J. Sound Vib. 295 (2006) 753–780.
[10] B. Ren, C.J. Lissenden, Ultrasonic guided wave inspection of adhesive bonds between composite laminates, Int. J. Adhes. Adhes. 45 (2013) 59–68.
[11] G. Zhao, B. Wang, T. Wang, W. Hao, Y. Luo, Detection and monitoring of delamination in composite laminates using ultrasonic guided wave, Compos. Struct. 225 (2019), 111161.
[12] A. Raghavan, C.E. Cesnik, 3-D elasticity-based modeling of anisotropic piezocomposite transducers for guided wave structural health monitoring, (2007).
[13] L. Yu, G. Bottai-Santoni, V. Giurgiutiu, Shear lag solution for tuning ultrasonic piezoelectric wafer active sensors with applications to Lamb wave array imaging, Int. J. Eng. Sci. 48 (2010) 848–861.
[14] S. Banerjee, C.B. Pol, Theoretical modeling of guided wave propagation in a sandwich plate subjected to transient surface excitations, Int. J. Solids Struct. 49 (2012) 3233–3241.
[15] W. Luo, J.L. Rose, Phased array focusing with guided waves in a viscoelastic coated hollow cylinder, J. Acoust. Soc. Am. 121 (2007) 1945–1955.
[16] D. Cerniglia, A. Pantano, N. Montinaro, 3D simulations and experiments of guided wave propagation in adhesively bonded multi-layered structures, NDT & E Int. 43 (2010) 527–535.
[17] B.I. Murat, P. Khalili, P. Fromme, Scattering of guided waves at delaminations in composite plates, J. Acoust. Soc. Am. 139 (2016) 3044–3052.
[18] W. Ostachowicz, P. Kudela, M. Krawczuk, A. Zak, Guided Waves in Structures For SHM: the Time-Domain Spectral Element Method, John Wiley & Sons, 2011.
[19] H. Michels, Abscissas and weight coefficients for Lobatto quadrature, Math. Comput. 17 (1963) 237–244.
[20] A. Żak, M. Krawczuk, W. Ostachowicz, Propagation of in-plane elastic waves in a composite panel, Finite Elem. Anal. Des. 43 (2006) 145–154.
[21] P. Kudela, M. Krawczuk, W. Ostachowicz, Wave propagation modelling in 1D structures using spectral finite elements, J. Sound Vib. 300 (2007) 88–100.
[22] F. Li, H. Peng, X. Sun, J. Wang, G. Meng, Wave propagation analysis in composite laminates containing a delamination using a three-dimensional spectral element method, Math. Probl. Eng. 2012 (2012).
[23] S.S. Lih, A.K. Mal, On the accuracy of approximate plate theories for wave field calculations in composite laminates, Wave Motion 21 (1995) 17–34.

[24] D.Roy Mahapatra, S. Gopalakrishnan, A spectral finite element model for analysis of axial–flexural–shear coupled wave propagation in laminated composite beams, Compos. Struct. 59 (2003) 67–88.
[25] P. Kudela, W. Ostachowicz, A multilayer delaminated composite beam and plate elements: reflections of Lamb waves at delamination, Mech. Adv. Mater. Struct. 16 (2009) 174–187.
[26] J. Moll, R. Schulte, B. Hartmann, C. Fritzen, O. Nelles, Multi-site damage localization in anisotropic plate-like structures using an active guided wave structural health monitoring system, Smart Mater. Struct. 19 (2010), 045022.
[27] S. He, C.T. Ng, A probabilistic approach for quantitative identification of multiple delaminations in laminated composite beams using guided waves, Eng. Struct. 127 (2016) 602–614.
[28] L. Wang, F. Yuan, Lamb wave propagation in composite laminates using a higher-order plate theory. Nondestructive Characterization For Composite Materials, Aerospace Engineering, Civil Infrastructure, and Homeland Security 2007, SPIE, 2007, pp. 137–148.
[29] J.M. Whitney, Shear correction factors for orthotropic laminates under static load, J. Appl. Mech. 40 (1973) 302–304.
[30] J. Zhao, H. Ji, J. Qiu, Modeling of Lamb waves in composites using new third-order plate theories, Smart Mater. Struct. 23 (2014), 045017.
[31] M. Jain, S. Kapuria, C1-continuous time-domain spectral finite element for modeling guided wave propagation in laminated composite strips based on third-order theory, Compos. Struct. 289 (2022), 115442.
[32] R. Schulte, C. Fritzen, J. Moll, Spectral element modelling of wave propagation in isotropic and anisotropic shell-structures including different types of damage, in: Proceedings of the IOP Conference Series: Materials Science and Engineering, IOP Publishing, 2010, 012065.
[33] K.Y. Jhang, Nonlinear ultrasonic techniques for nondestructive assessment of micro damage in material: a review, Int. J. Precis. Eng. Manuf. 10 (2009) 123–135.
[34] D. Broda, L. Pieczonka, V. Hiwarkar, W. Staszewski, V. Silberschmidt, Generation of higher harmonics in longitudinal vibration of beams with breathing cracks, J. Sound Vib. 381 (2016) 206–219.
[35] R. Guan, Y. Lu, K. Wang, Z. Su, Fatigue crack detection in pipes with multiple mode nonlinear guided waves, Struct. Health Monit. 18 (2019) 180–192.
[36] C. Rekatsinas, D. Saravanos, A hermite spline layerwise time domain spectral finite element for guided wave prediction in laminated composite and sandwich plates, J. Vib. Acoust. 139 (2017).
[37] N. Nanda, S. Kapuria, S. Gopalakrishnan, Spectral finite element based on an efficient layerwise theory for wave propagation analysis of composite and sandwich beams, J. Sound Vib. 333 (2014) 3120–3137.
[38] M. Jain, S. Kapuria, S. Pradyumna, Efficient time-domain spectral element with zigzag kinematics for multilayered strips, Int. J. Mech. Sci. 232 (2022), 107603.
[39] M.K. Pandit, A.H. Sheikh, B.N. Singh, An improved higher order zigzag theory for the static analysis of laminated sandwich plate with soft core, Finite Elem. Anal. Des. 44 (2008) 602–610.
[40] A. Chakrabarti, H. Chalak, M.A. Iqbal, A.H. Sheikh, A new FE model based on higher order zigzag theory for the analysis of laminated sandwich beam with soft core, Compos. Struct. 93 (2011) 271–279.
[41] H.D. Chalak, A. Chakrabarti, M.A. Iqbal, A.H. Sheikh, An improved C0 FE model for the analysis of laminated sandwich plate with soft core, Finite Elem. Anal. Des. 56 (2012) 20–31.
[42] R.C. Averill, Y.C. Yip, Thick beam theory and finite element model with zig-zag sublaminate approximations, AIAA J. 34 (1996) 1627–1632.
[43] K.J. Bathe, Finite element procedures, Klaus-Jurgen Bathe, 2006.
[44] J.N. Reddy, Mechanics of Laminated Composite Plates and shells: Theory and Analysis, CRC Press, 2003.
[45] A.K. Chopra, Dynamics of structures: Theory and Applications to Earthquake Engineering, 3rd ed. ed., Pearson/Prentice Hall, Upper Saddle River, N.J, 2007.
[46] S. Duczek, H. Gravenkamp, Mass lumping techniques in the spectral element method: on the equivalence of the row-sum, nodal quadrature, and diagonal scaling methods, Comput. Methods Appl. Mech. Eng. 353 (2019) 516–569.
[47] P. Aryan, A. Kotousov, C.T. Ng, B. Cazzolato, A model-based method for damage detection with guided waves, Struct. Control Health Monit. 24 (2017) e1884.
[48] A. Huber, Dispersion calculator, 2018.
[49] A.K. Barouni, D.A. Saravanos, A layerwise semi-analytical method for modeling guided wave propagation in laminated and sandwich composite strips with induced surface excitation, Aerosp. Sci. Technol. 51 (2016) 118–141.
[50] C. Rekatsinas, C. Nastos, T. Theodosiou, D. Saravanos, A time-domain high-order spectral finite element for the simulation of symmetric and anti-symmetric guided waves in laminated composite strips, Wave Motion 53 (2015) 1–19.
[51] D. Alleyne, P. Cawley, A two-dimensional Fourier transform method for the measurement of propagating multimode signals, J. Acoust. Soc. Am. 89 (1991) 1159–1168.
[52] C. Ramadas, K. Balasubramaniam, A. Hood, M. Joshi, C. Krishnamurthy, Modelling of attenuation of Lamb waves using Rayleigh damping: numerical and experimental studies, Compos. Struct. 93 (2011) 2020–2025.
[53] C. Ramadas, K. Balasubramaniam, M. Joshi, C.V. Krishnamurthy, Interaction of guided Lamb waves with an asymmetrically located delamination in a laminated composite plate, Smart Mater. Struct. 19 (2010).
[54] V.K. Chillara, C.J. Lissenden, Review of nonlinear ultrasonic guided wave nondestructive evaluation: theory, numerics, and experiments, Opt. Eng. 55 (2016), 011002.
[55] R. Soleimanpour, C.T. Ng, C.H. Wang, Higher harmonic generation of guided waves at delaminations in laminated composite beams, Struct. Health Monit. 16 (2017) 400–417.